(1)

UNCLASSIFIED

SECURITY CLASSIFICATION OF THIS PAGE (When Data Entered)

REPORT DOCUMENTATION PAGE

READ INSTRUCTIONS BEFORE COMPLETING FORM

1. REPORT NUMBER: AFIT/CI/NR 88- 10
2. GOVT ACCESSION NO.
3. RECIPIENT'S CATALOG NUMBER

4. TITLE (and Subtitle): SEARCH FOR WAVE INDUCED PARTICLE PRECIPITATION FROM LIGHTNING AND TRANSMITTER SOURCES
5. TYPE OF REPORT & PERIOD COVERED: MS THESIS
6. PERFORMING ORG. REPORT NUMBER

7. AUTHOR(s): JON ERIC LUNDBERG
8. CONTRACT OR GRANT NUMBER(s)

9. PERFORMING ORGANIZATION NAME AND ADDRESS: AFIT STUDENT AT: UNIVERSITY OF MARYLAND
10. PROGRAM ELEMENT, PROJECT, TASK AREA & WORK UNIT NUMBERS

11. CONTROLLING OFFICE NAME AND ADDRESS
12. REPORT DATE: 1988
13. NUMBER OF PAGES: 110

14. MONITORING AGENCY NAME & ADDRESS (if different from Controlling Office): AFIT/NR, Wright-Patterson AFB OH 45433-6583
15. SECURITY CLASS. (of this report): UNCLASSIFIED
15a. DECLASSIFICATION/DOWNGRADING SCHEDULE

16. DISTRIBUTION STATEMENT (of this Report): DISTRIBUTED UNLIMITED: APPROVED FOR PUBLIC RELEASE

17. DISTRIBUTION STATEMENT (of the abstract entered in Block 20, if different from Report): SAME AS REPORT

18. SUPPLEMENTARY NOTES: Approved for Public Release: IAW AFR 190-1
LYNN E. WOLAVER Lynn Wolaver 12 Feb 88
Dean for Research and Professional Development
Air Force Institute of Technology
Wright-Patterson AFB OH 45433-6583

19. KEY WORDS (Continue on reverse side if necessary and identify by block number)

20. ABSTRACT (Continue on reverse side if necessary and identify by block number): ATTACHED

DD FORM 1 JAN 73 1473 EDITION OF 1 NOV 65 IS OBSOLETE

UNCLASSIFIED

SECURITY CLASSIFICATION OF THIS PAGE (When Data Entered)

ABSTRACT

Title of Thesis: A Search for Wave Induced Particle Precipitation from Lightning and Transmitter Sources

Jon Eric Lundberg, Master of Science, 1988

Thesis directed by: Dr. Theodore J. Rosenberg, Professor, Institute for Physical Science and Technology

Wave induced particle precipitation is introduced and examined for whistlers whose sources are within the plasmapause. The possible correlation between lightning strokes that carry positive charge to the ground and the observed "Trimpi" events is discussed, sudden phase and/or amplitude shifts of a received VLF signal with gradual return to predisturbed values. The thunderstorm charging mechanisms that lead to the observed charge distribution and the advection of the positively charged cirrus anvil away from the body of the thunderstorm are briefly examined. The comparative current strengths and the relative frequency of positive and negative strokes is studied for different types of thunderstorms. The magnetospheric ducting of the lightning-generated whistler wave and the interaction with trapped electrons is examined. The detectable effects the precipitating electrons have on the ionosphere is introduced. The Wave Induced Particle Precipitation campaign, conducted between 15 July and 1 August 1987 at Wallops Island. The instrumentation involved in the campaign is highlighted,

with the University of Maryland participation emphasized. Included are testing and design of the x-ray detector and balloon launch considerations. The problems encountered during the x-ray detector's balloon flights are examined. The riometer and x-ray detector data analysis methods are mentioned. The results were negative for the data that was analyzed but the limiting factors severely restricted the usable data. Possible experimental methods are mentioned. (Theses; 121)

A SEARCH FOR WAVE INDUCED PARTICLE PRECIPITATION FROM LIGHTNING AND TRANSMITTER SOURCES

by

Jon Eric Lundberg

Thesis submitted to the Faculty of the Graduate School
of The University of Maryland in partial fulfillment
of the requirements for the degree of
Master of Science
1988

Advisory Committee:
Professor Theodore Rosenberg
Associate Professor Robert Ellingson
Assistant Professor George Huffman

ACKNOWLEDGEMENTS

I would like to thank my wife, Debbie for her help and support. The many other people that helped with this project were; Peter Hammer, who gave invaluable assistance with the figure preparation and helped me print this thesis at his office. Dr. Rosenberg, who gave his guidance and singlehandedly taught me what I know of the upper atmosphere. Dr. Sumant Krishnaswamy and Tilak Hewagama supplied the computer programming expertise. Dr. David Matthews, Dan Detrick, Larry Lutz, Qian Wu, and John Paquette were all willing to drop what they were doing and answer my questions. Further support was provided by the National Science Foundation under grant ATM 861508.

TABLE OF CONTENTS

LIST OF TABLES

LIST OF FIGURES

CHAPTER 1

INTRODUCTION

LINKS BETWEEN REGIONS

The wave induced particle precipitation process crosses many of the traditional lines of separation between geophysical disciplines. Figure 1 shows a schematic of the atmospheric regions involved in the wave induced particle precipitation process. Tropospheric lightning produces a wave that penetrates the ionosphere. The wave propagates through the magnetosphere and interacts with magnetospheric electrons. The electrons may precipitate into the ionosphere, and increase the local ionization level.

Wave Induced Particle Precipitation involves a wide variety of scale sizes and physical principles. The wave-particle interactions take place several earth radii away from the Earth's surface. Cloud to ground lightning strokes, which trigger the electron precipitation, directly impact the ground. The behavior of the entire Earth's magnetosphere comes into play, as does the interaction of a single radio photon with an individual electron.

The physics involved range from conditional

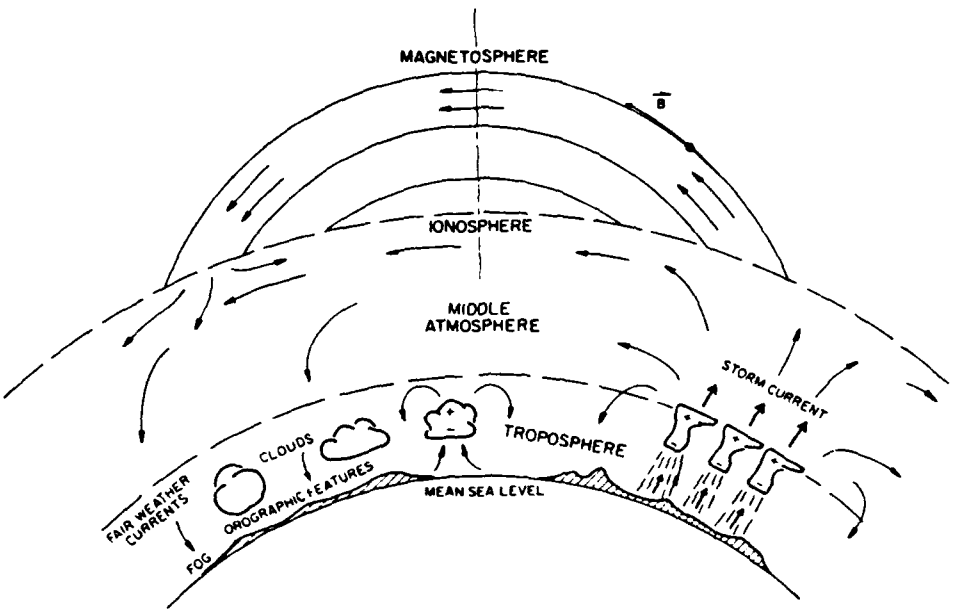

Figure 1. The Global Electrical Circuit. (From *The Earth's Electrical Environment*)

instability producing convection, the motion of charged particles in an electric field, the motions of electrons in a magnetic field, to the interactions between energetic eletrons and upper atmospheric gasses. All of this activity is taking place in portions of the atmosphere ranging from the boundary layer to a body of plasma at densities so low that the definition of thermodynamic temperature and pressure are somewhat meaningless.

THE TROPOSPHERE

The laws of fluid dynamics dominate the motions of the troposphere. The background electric field will come into play only on the smallest scale. The motions of free ions and of ions within a water droplet are affected by the electric field as will be seen in Chapter 2, but the mean free path of a free electron in the troposphere is so short that there is little ionization relative to the upper regions of the atmosphere [Panel on the Earth's Electrical Environment, Hoppel et al. 1983].

THE IONOSPHERE

The ionosphere lies between the magnetosphere and the stratosphere (Figure 2). The ionization levels present are intense enough to affect the propagation of radio waves, but the motions of the particles are not controlled by the magnetic field. A complex mixture of fluid

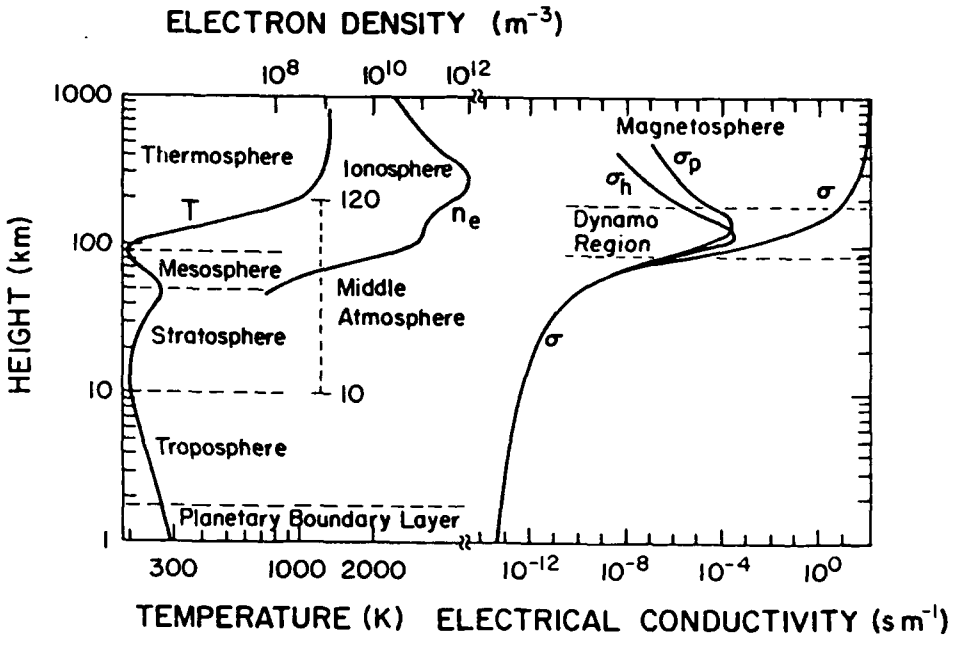

Figure 2. Vertical Profile of the Atmosphere to 1000km. The lower magnetosphere merges into the upper ionosphere. (From *The Earth's Electrical Environment*)

dynamics of low density gasses and motions of currents in a magnetic field control the behavior of the ionosphere [Panel on the Earth's Electrical Environment, Krider et al. 1983]. The lower edge of the ionosphere is generally around 60km [Panel on the Earth's Electrical Environment, Reid 1983], while the upper edge is hard to separate from the lower magnetosphere.

The ionosphere plays a part in all stages of the current study. The fair weather electric field (Figure 3) produced by the voltage difference between the ionosphere and the Earth's surface is instrumental in the initial charging of a thunderstorm. The sferics emitted by the lightning channel see the Earth-Ionosphere system as a waveguide until the sferic passes upwards through the ionosphere on its way to precipitating electrons back into the ionosphere.

THE MAGNETOSPHERE

The magnetosphere is defined as the region where the motion of charged particles is dominated by the magnetic field [Lanzerotti and Park 1978]. The magnetosphere extends roughly down to 100km, the outer limit of the magnetosphere will range from ten earth radii in the direction of the sun to sixty earth radii away from the sun (Figure 4). Most of the particles in the magnetosphere are charged. They are either free electrons

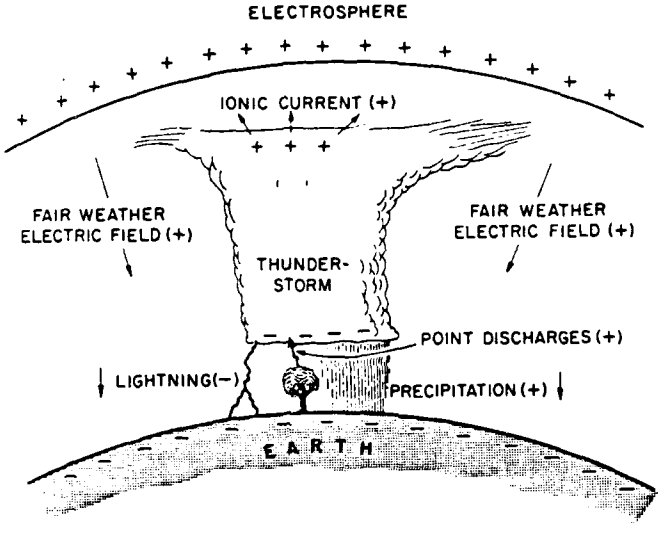

Figure 3. Lower Atmospheric Electric Field. Arrows indicate current flow, positive and negative signs indicate polarity of the flow. (From *The Earth's Electrical Environment*)

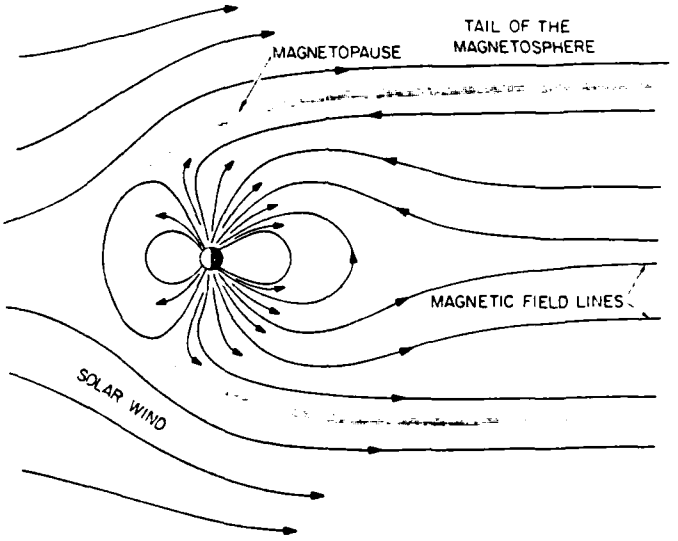

Figure 4. The Magnetosphere. Cross-section of the magnetosphere. (From Hargreaves, *The Upper Atmosphere and Solar Terrestrial Relations*, 1979)

or ionized atoms, and constitute a plasma. The particle densities are so low that the recombination rate is in rough equilibrium with the ionization due to sunlight [Hargreaves 1979].

Figure 5 depicts the magnetosphere in greater detail, the plasmasphere and the plasmapause. The plasmasphere is an area of higher particle densities, while the plasmapause is a region where the electron density will drop by approximately two orders of magnitude across a relatively short distance [Hargreaves 1979]. This plasmasphere is relatively stable and sees less interaction with magnetospheric perturbations and the solar wind.

The lightning-related precipitation studied lies well within the plasmasphere, measured from an L-shell of around 2.5. An L-shell is defined as the distance away, in earth radii, from the Earth's center that a magnetic field line would be when it was over the equator, if the magnetic field was a perfect dipole. The field lines of Figure 4 clearly show this to be somewhat inadequate for high latitudes. The definition has some merit for the plasmasphere. The plasmapause lies roughly around an L-shell of 4 [Hargreaves 1979].

THE WAVE PARTICLE INTERACTION

Lightning produces a powerful electromagnetic wave.

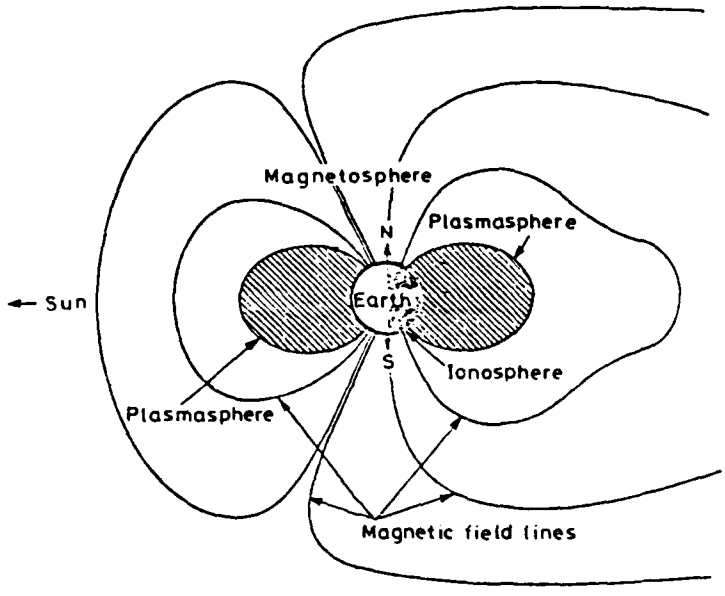

Figure 5. The Plasmasphere. Cross-section showing the plasmasphere in relation to the magnetosphere. (From Hargreaves, *The Upper Atmosphere and Solar Terrestrial Relations*)

The higher frequencies of the wave are rapidly absorbed by the troposphere. The Very Low Frequency (VLF) radio waves are reflected by the ionosphere and the Earth's surface.

These waves may propagate great distances in the lower atmosphere (troposphere and stratosphere). The VLF radio waves also may penetrate the ionosphere and pass into the magnetosphere if the angle of incidence and the ionospheric index of refraction permit. The index of refraction is a function of the charge density distribution. A lower ionization level will allow more waves to pass through.

Most of the waves that enter the magnetosphere will dissipate. Some of the waves may follow a geomagnetic field line. This occurs if the field line has a local charge density distribution such that the line effectively acts as a waveguide along its length.

The guided VLF radio waves may interact with electrons that are following the same field line. The electron will be less tightly bound to the field line if the electron losses energy to the wave in the interaction. An electron that is less tightly bound the field line is less likely to be reflected by the ionosphere back into the magnetosphere. The electrons that are not reflected precipitate into the ionosphere.

Electrons lose energy when they interact with the upper ionosphere, principally due to ionization of

atmospheric constituents, and the production of Bremsstrahlung x-rays. Of the two the vast majority of the electron's energy goes into ionization [Berger and Seltzer 1972].

The wave particle interaction is not specific to waves generated by lightning. VLF radio transmitters are also thought to produce electron precipitation within the plasmasphere. VLF waves produced within the magnetosphere will also produce precipitation, but at higher latitudes than are under investigation here [Rosenberg et al. 1987].

PREVIOUS INVESTIGATIONS

The wave particle interaction and the effect of the electron precipitation on the ionosphere are similar at all latitudes. The highly energetic particle fluxes associated with auroral activity produce many of the same signatures that the electron fluxes produced by the wave particle interaction generate.

The electron flux, Bremsstrahlung x-rays and increased ionization are observable through a variety of methods. A rocket borne particle detector may directly observe a burst of electrons [Goldberg et al. 1987]. The magnetic perturbations due to the current flow into the upper ionosphere may be detected by ground-based micropulsation magnetometers. The bremsstrahlung x-rays may be detected from balloon-borne x-ray detectors

[Rosenberg et al. 1987]. The ionization may be detected with photometers, which detect photons given off during recombination. Increased ionization will also produce detectable pertubations of VLF waves as they propagate past the precipitation region [Inan and Carpenter 1987].

The only methods that have detected precipitation within the plasmasphere are rocket based [Goldberg et al. 1987], and the "Trimpi" effect on the propagation of radio waves, sudden phase and/or amplitude shifts with gradual return to predisturbed values [Inan and Carpenter 1987]. The methods used by the various investigators during the Wave Induced Particle Precipitation campaign will be discussed further in Chapter 4.

SUMMARY

The wide range of processes involved in wave particle interactions defies a thorough discussion of each interaction within the scope of this study. Thunderstorm charging and a brief discussion of lightning will introduce the subject. A general development of the wave particle interaction and the effect of the precipitation on the ionosphere follow.

The instrumentation and detection methods involved in the Wave Induced Particle Precipitation (WIPP) campaign are discussed in Chapter 4. The events of the campaign and the University of Maryland participation will follow

in Chapter 5. Chapter 6 concludes with a discussion of the results of the experiment.

The production of the thunderstorm charge distribution and its effects on lightning polarity are highlighted due to the apparent correlation between positive lightning strokes and Trimpi events that Dr. Kintner of Cornell had seen, and discussed during science meetings during the WIPP campaign.

CHAPTER 2

THUNDERSTORM CHARGING AND LIGHTNING

THUNDERSTORM INTRODUCTION

We now briefly review some of the more pertinent aspects of thunderstorms in order to properly associate one class of Wave Induced Particle Precipitation to its origin in a lightning bolt. Thunderstorms are latent heat driven convective cells. The electrical effects are a consequence of the dynamics of the storm rather than being the driving force of the cell. The processes that create a strong thunderstorm do, however, enhance the charging of the thunderstorm.

The ideal situation for strong thunderstorm development is moist, conditionally unstable air over a fairly deep section of the troposphere in addition to a synoptic to sub-synoptic scale forcing. This forcing may be supplied by a terrain feature such as flow up a slope, a frontal system or a coastal front. The positive bouyancy of the lower-level air forces it to rise and to cool dry-adiabatically. The cooling will eventually cause the rising air to reach saturation and start condensing out liquid water. The condensation releases latent heat, which increases the instability of the rising air in

conditional instability, producing continued vertical acceleration of the rising air parcel until a more stable region of the troposphere is reached. Many thunderstorms eventually reach the tropopause and penetrate a small distance into the highly stable stratosphere. As the thunderstorm builds, it condenses large amounts of moisture into liquid water which accumulates in increasingly large droplets.

Once the vertical motion starts air will be supplied by continuity to the base of the thunderstorm. This recently supplied air will see the same forcing as the air it replaces since this air will also be statically unstable and moist. An updraft will form and push warm, moist air into the base of the thunderstorm. Energy will continue to be fed into the thunderstorm until the surroundings have been altered by the downdraft that forms to balance the updraft, and by the cooling due to evaporating precipitation.

Strong and severe thunderstorms require a downdraft that does not affect the incoming air. Such would be the case if the thunderstorm in Figure 6 were moving from left to right across the page. The updraft is coming from unmodified air, while the downdraft of cool, dry air is entering a region already cooled by precipitation. The surface intersection of these two drafts serves to produce strong convergence and will further accelerate the

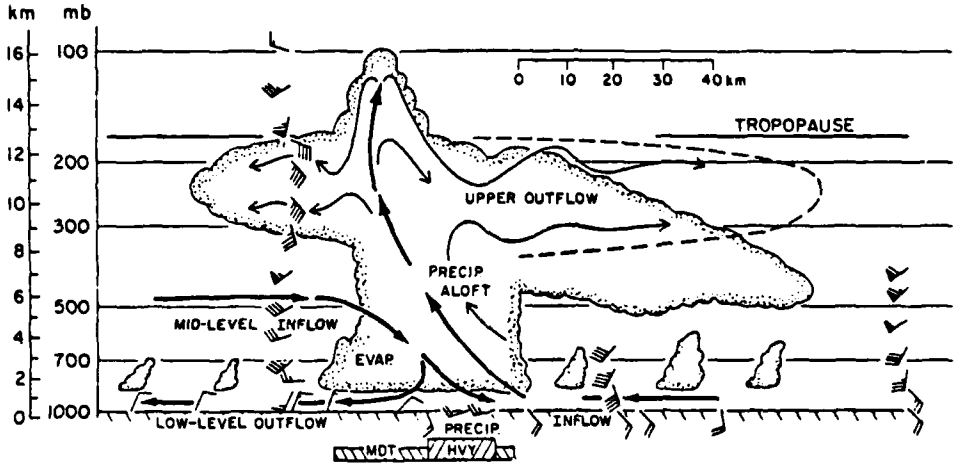

Figure 6. Thunderstorm Cross-Section. Cross-section of a squall line thunderstorm. Winds are shown relative to the thunderstorm. Arrows are streamlines, with thickness indicating strength of flow. (From *The Earth's Electrical Environment*)

incoming updraft.

The generally strong winds in the upper troposphere tend to spread out the upper reaches of the thunderstorm. This high-level spread is most pronounced in strong to severe thunderstorms and the later stages of average strength thunderstorms. Stronger thunderstorms tend to form in areas of strong vertical wind shear; older thunderstorms have had more time for the existing wind shear to act.

The mechanical processes that are responsible for a thunderstorm's kinetic energy are indirectly responsible for charging the thunderstorm. The increase in droplet interactions due to a broad spectrum of droplet sizes drives the charging process, but the droplet spectrum is a function of the available moisture and the conditional instability. A thunderstorm would merely be a strong rainshower if it were not for the charging processes and subsequent lightning.

The charging processes will usually only be able to produce sufficient charge once ice particles have formed at the top of the updraft. The release of latent heat is the driving force, but the availability of a wide range of droplet sizes allows much more interaction as the larger droplets have higher net downwards acceleration due to less wind resistance.

The vertical growth of the thundercloud past the

level of the -20°C isotherm is crucial both to the kinetic and electrical energy of the thunderstorm. The growth of ice particles into hailstones increases the intensity of rain. The formation of ice particles and small hailstones is a critical stage in the charging. A stronger updraft will allow larger droplets to remain within the cloud, while very strong updrafts will allow large hailstones to grow at heights above the -20°C isotherm, increasing the range of droplet/ice particle sizes. The broader spread of the droplet size distribuation increases the rate of particle interaction. The droplets are equally attracted by gravity, but the viscous force holding the drop up is a function of the ratio between the mass and the surface area. The mass is a function of the cube of the droplet radius, while the area is a function of the square of the radius. Thus, the viscous force falls off as the droplet mass increases.

THUNDERSTORM CHARGING MECHANISMS

Charge separation in thunderstorms works to increase net negative charge in the lower and middle regions of the thunderstorm, while creating a small positive charge at the base, and a larger positive charge at the top of the cloud [Figure 7]. There are a variety of mechanisms that create this charge distribution. The charging tends to be on the individual ion level while the storm is a

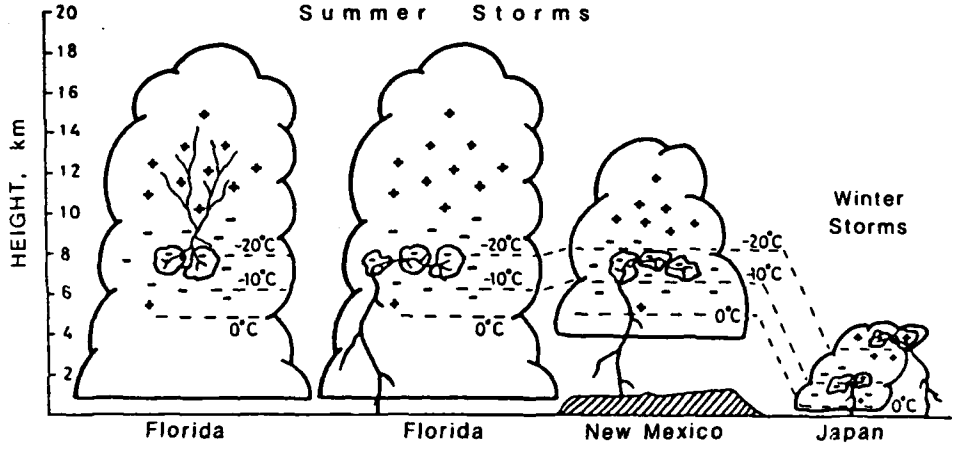

Figure 7. Thunderstorm Charge Distribution. Net charge is shown for each region as a positive or negative sign. The charge distribution seems highly correlated with temperature rather than height. (From *The Earth's Electrical Environment*)

nonprecipitating convective cloud, termed the cloud stage charging processes.

The first of the ion level mechanisms is diffusion charging. The full form of the solution of ion motion includes diffusion due to random motion in a nonuniform density field, bulk motion of the air, and motion of the ions due to the background electric field. Diffusion charging assumes the bulk motion of the air and the background electric field to be small. The droplet capture of the ions is purely due to diffusion. Ions colliding with cloud droplets will be added to the droplet. Diffusion charging greatly reduces the free air ion density [Panel on the Earth's Electrical Environment, Beard and Ochs, 1983), and is the dominant process producing droplet charge distribution in nonconvective clouds and the early stages of thunderstorms.

The growing cloud increases its electric field through diffusion charging. If the cloud is a growing convective storm, a surface updraft will form to replace vertically accelerated air. Drift charging works to move ion charge to cloud droplets under these circumstances. Both the flux of ions moving with the electrically neutral air and motion of the ions due to the background electric field influence drift charging. Drift charging further reduces the free ion concentration in the cloud. The surroundings of the cloud will be stripped of much of its

free ions under the electric field attraction of drift charging.

The last of the cloud stage charging mechanisms is active when there is relative movement between cloud droplets and ions. Droplet sizes of greater than four microns will be polarized and will selectively gather negatively charged ions in the slow moving case as seen in Figure 8. The ions are moving more slowly in the electric field than the droplets are falling against the viscous effects. The current produced by this effect is only one-sixth of the current from drift charging(Panel on the Earth's Electrical Environment, Beard and Ochs, 1983). The importance of this effect lies more in its selectivity than its magnitude, since it tends to give small cloud droplets a net negative charge.

Through the non-precipitating cloud stage, the effect of the droplet charging has been to remove ions from the air surrounding the droplets, and due to drift charging, the region surrounding the cloud. These effects are fairly localized and little vertical differentiation takes place until the formation of raindrops. As the nascent thunderstorm grows, the size of the droplets increases. The range of the sizes also increases, thus allowing significant relative motion between different size droplets. As a droplet reaches the size where it can no longer be supported by the viscous forces, it falls with

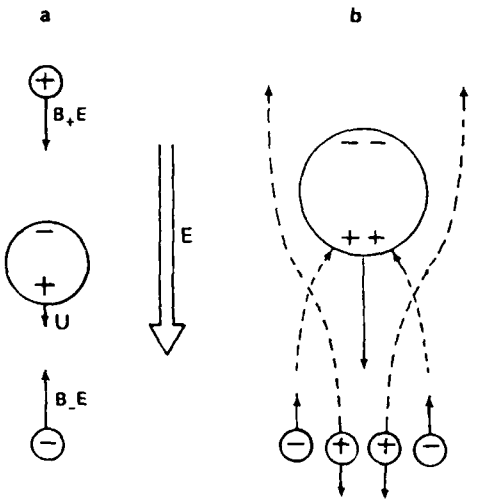

Figure 8. Selective Ion Capture. Droplet charging due to ions gathered through droplet polarization. (a) fast ions, ions moving much faster than the neutral air; (b) ions moving slower than the neutral air. (From *The Earth's Electrical Environment*)

gravity against the air flow, coming into contact with smaller drops being carried upwards.

The rain stage begins once the droplets are big enough to have vertical relative motions. Both charging mechanisms of the rain stage involve collisions between droplets. The first of these is breakup charging. When small droplets, those less than one tenth of a millimeter diameter, collide they tend to merge into a larger droplet. A collision between raindrops (1-6mm) may create a number of smaller droplets as the force of the impact sets up instabilities in the raindrop. These instabilities overcome the surface tension, producing the breakup. The breakup of the raindrop takes place much more slowly than the movement of the charges within the drop. If the droplet is stretched vertically, it will readjust its polarization before breaking up. The resulting smaller droplets will each be left with an excess of either negative or positive charge (Figure 9). This process seems to have little effect on the overall field [Panel on the Earth's Electrical Environment, Beard and Ochs 1983], but probably is a major source of droplet charging.

Two colliding drops may exchange charge if they do not merge. This induction charging seems to be the major mechanism for the large vertical charge separation, at least before the ice processes are involved [Panel on the

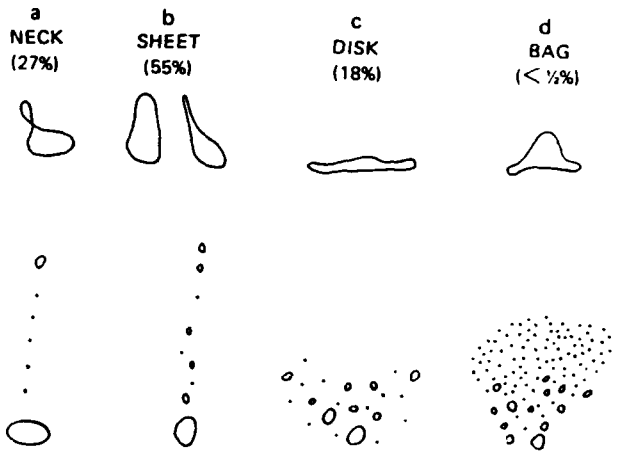

Figure 9. Breakup Charging. Four observed breakup patterns. (From *The Earth's Electrical Environment*)

Earth's Electrical Environment, Beard and Ochs 1983]. Figure 10 demonstrates induction charging between a large drop and a small drop which come into contact. The large drop will pick up a negative charge and the small drop a positive charge. Induction charging feeds back on the background electric field. The small drop continues to be carried upwards relative to the large drop. The background field is reinforced (Figure 2) by the differentiation of vertically mobile charges. The stronger background field will increase droplet polarization and increase the efficiency of all of the interactions discussed so far. However, the interactions to this point in the precipitating cloud have yet not produced the charge separation required to produce lightning.

A wider variety of processes comes into play once the cloud builds past the freezing level, especially after the cloud reaches the height of the -20°C isotherm. Induction charging of liquid droplets and ice particles continues to play a role, but the major charging mechanism comes from the interaction of large frozen graupel and smaller supercooled water droplets. Above the -20°C isotherm, small hail pellets form and will grow if the updraft is sufficient to hold them up against gravity.

A thermoelectric effect is produced by the temperature gradient across the interface between the ice

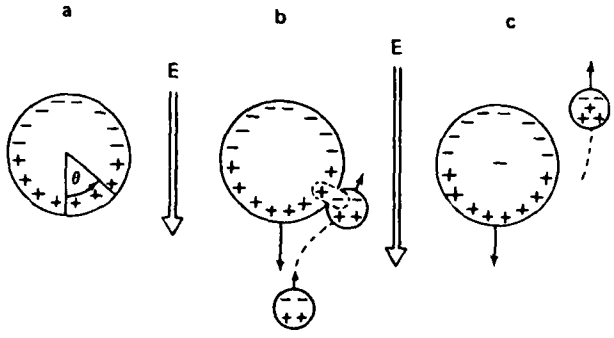

Figure 10. Induction Charging. Induction charge transfer in a downward directed field: (a) incoming drops are polarized; (b) droplet collision, though the drops do not coalesce; (c) net charge has changed for each droplet. (From *The Earth's Electrical Environment*)

pellet and the droplet. The ice has been warmed as previous droplets froze onto its surface. The ice pellet might be warmer than a supercooled water droplet by as much as 10°C. The charge transferred in any one interaction will be quite small, but the growing ice pellet will collide with many droplets.

Freezing potentials due to chemical impurities in droplets that impact and freeze onto the hailstone also are a significant contributor to hailstone charging. The dissolved salts and other impurities leach into the ice, carrying a relatively high proportion of the droplet's ions with them.

Once this hail stage is reached, the background electric field is no longer a controlling factor. The charging due to freezing potentials and the thermoelectric effect are both independent of the electric field, and are now the major contributors to the thunderstorm charge.

The charging mechanisms can be summed up as having two major classes. The mechanisms of the building thunderstorm, which are dependent on the background electric field, and the mechanisms of the thunderstorm, which are independent of the field. The importance is that the building thunderstorm charging rate is dependent upon the electric field, while the thunderstorm charge grows at a rate determined by the parameters that cause the ice pellets to grow. This is determined by the

continuing supply of moisture and the strong updraft, which keeps the hailstone aloft. Both the rain stage and thunderstorm stage charging processes do reinforce the field strength, and this reinforces the building thunderstorm charging processes which continue to contribute to the overall charge, especially below the -20°C level.

The effect of the various charging mechanisms is to produce a diffuse net positive charge in the cirrus anvil, a region of dense negative charge in the main body, and a weak positive charge at the base and in the precipitation of the thunderstorm. The fair weather electric field is normally around 100 and 200 V/m, under a thunderstorm the field may become as high as 10,000 V/m (*Panel on the* Earth's Electrical Environment, Krehbiel 1983).

The anvil charge is produced by small droplets and ice crystals that have given some of their negative charges to larger raindrops through the induction charging process, in return picking up positive charge, and so are left with net positive charge. The large drops are carried lower in the thunderstorm, while the positively charged droplets are carried up to the highest regions of the thunderstorm. If the droplet was not already frozen, the extreme cold of the thunderstorm cloudtop soon freezes even the purest liquid water drop. The average environmental winds at the anvil level are much greater

than the speed of the main body of the thunderstorm, and so the positively charged anvil is carried away from the main body of the thunderstorm.

The main body of the thunderstorm is much more active than the upper portions of the thunderstorm. In the precipitation region the charge distribution is reversed. The large raindrops are positively charged, while the negative charge remains in the thundercloud, so the precipitation carries positive charge to the ground. The high negative charge density produced must be reduced, an action accomplished through lightning.

LIGHTNING

Once the field within the thunderstorm becomes high enough, it can create a current. This current can flow from cloud to cloud, and from cloud to ground. The origin of most lightning is within the highly negatively charged main trunk of the storm.

The details of the current flow have seen much research. The primary difficulty in studying lightning has been the unpredictability of the location and timing of both the thunderstorm and lightning. The lightning starts as a series of short, connected pulses that each span a small portion of the eventual length of the lightning bolt (Figure 11). These stepped leaders carry the ionized wave towards the surface. Electrical contact

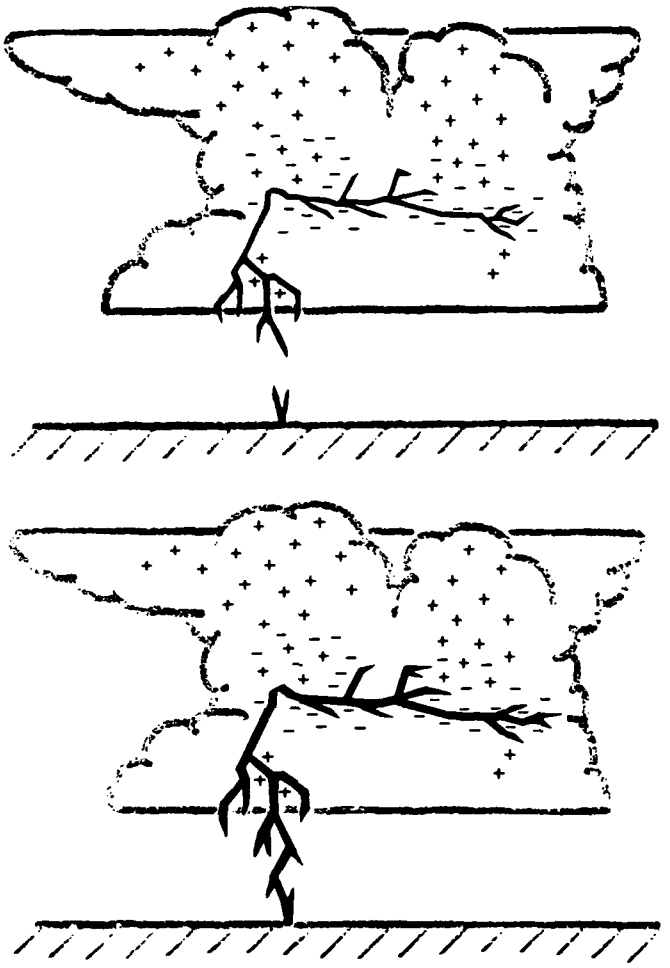

Figure 11. Stepped Leader. (a) charge is starting to flow from the surface to meet the stepped leader. (b) the return stroke flows along the path where the surface charge met one of the fingers of the stepped leader. (From *The Earth's Electrical Environment*)

is usually made with the surface the stepped leader extending to the ground. Contact may also occur if charge surges upwards from the ground to the stepped leader. The stepped leader usually carries a wave of negative ions to the surface and leaves a highly ionized path that serves as a good conductor for subsequent strokes. The more energetic return stroke will surge up from the surface along the path of the stepped leader once contact is made. The return stroke is usually positively charged. Several repetitions of current flow from cloud to ground with return strokes from ground to cloud usually follow. Each stroke will discharge a different portion of the cloud, but will follow the same path between the cloud base and the ground (Panel on the Earth's Electrical Environment, Krehbiel 1983). The combination of negative flow to the ground and positive flow to the cloud reduces the negative charge in the central section of the cloud.

The intracloud bolts are similar to the cloud to ground bolts but carry charge within the cloud, redistributing charge internally. The intracloud bolts generally carry negative charge upwards, into the cirrus anvil. These bolts can be seen from the ground to dimly illuminate the cloud.

The cloud to ground lighting bolts (CG) are more powerful than the intracloud bolts, and can be further divided into carriers of negative charge to the ground and

the more uncommon carriers of positive charge [Panel on the Earth's Electrical Environment, Krehbiel 1983]. The positive cloud to ground flashes are the more powerful of the CG strokes. The average current carried is generally an order of magnitude higher than the negative CG strokes [Beasley 1983].

Another difference between positive and negative CGs is that a series of strokes is unusual in the positive CGs. There seems to be substantial intracloud lightning as a precurser to the cloud to ground strokes. This appears to concentrate the positive charge in one portion of the cirrus anvil. The positive CGs thus have a single return stroke of longer duration that discharges the concentrated charge [Beasley 1983]. The positive CGs are also frequently originate from within the positively charged cirrus anvil. Most of the charge imbalance within the cirrus anvil is usually readjusted by intracloud strokes as seen in Figure 12, parts a, c, and e. The unusual positive strokes are more common if the cirrus anvil is advected away from the body of the thunderstorm. Since this will occur more frequently in older or severe thunderstorms [Orville 1988], the frequency of positive strokes is higher within these types of thunderstorms. The positive strokes come from the spread out anvil and are scattered over a wide region [Orville 1988]. The negative strokes tend to originate from the central body

of the thunderstorm, and are concentrated within a small region.

Lightning reduces the charge imbalances produced by the charging mechanisms, which continue to build the imbalances as long as the storm is receiving energy from the updraft. Eventually both the electrical and kinetic energy of the storm are dissipated.

An additional effect of the lightning is to produce a powerful elecromagnetic signal that propagates across large distances along the Earth's surface. This signal will be seen to be of vital interest in the study of wave-induced particle precipitation.

CHAPTER 3

THE WAVE MAGNETOSPHERE INTERACTION

NATURAL WAVEGUIDES

The majority of the energy in a lightning stroke is the flow of the current. A portion heats the lightning channel to a peak temperature of 30,000K [Panel on the Earth's Electrical Environment, Krider 1983]. An electromagnetic wave is produced by the lightning channel, with an easily visible flash of light.

The lightning flash is a broad spectrum signal. The atmosphere is an efficient absorber for infrared (wavelengths from millimeters to micrometers) and ultraviolet waves (wavelength less than .4 micrometers), and these wavelengths are rapidly absorbed. Visible light is transmitted well through the depth of the atmosphere. Cloud to ground lightning is transmitted into the densest layer of the atmosphere. This layer is highly populated with particulate matter [Wallace and Hobbs 1979] and has the highest water vapor density. These additions to the free atmosphere are the most effective absorbers of visible light [Liou 1980]. The long path length through the dense lower atmospheric layers also increases the absorption of the shorter wavelengths.

A further limitation on the distance from the source that electromagnetic waves can be observed from the ground is the curvature of the earth. Any waves that are not reflected from some layer in the atmosphere or absorbed by the surface will pass into space within 100km from geometrical considerations alone. The Extremely Low Frequency (ELF), frequencies between .3 and 3kHz, and Very Low Frequency (VLF), frequencies between 3 and 30 kHz, radio waves are transmitted well by the atmosphere and are largely reflected by the Earth Ionosphere Waveguide. The wave guide effect is caused by relatively high charging of the Earth and Ionosphere with respect to the intervening atmosphere.

These radio waves easily propagate thousands of kilometers from the source region [Tolstoy, et. al. 1986] (Figure 13), and can be heard as radio static at substantial distances from any thunderstorm activity. The strength of the wave will decrease with the inverse square law of distance from the source, but the high energy of the broadcast wave can still produce a signal at great distances. The peak electromagnetic power radiated by a lightning bolt has been estimated as three to five billion watts, with the energy in the visible portion only in the tens of megawatts [Krider and Guo 1983]. The lightning electromagnetic wave, termed sferic, has ample energy available in the low frequency ranges.

Depending on irregularities of the ionosphere that cause failure of the waveguide effect, the ULF and VLF waves will pierce the ionosphere and pass up into the magnetosphere. The majority of the waves that do so are eventually lost due to the combined effects of the wave passing out to space and absorption. A minority of the waves can become "ducted" and are the waves of interest in this study.

Magnetospheric ducting occurs if a wave is reflected each time it starts to diverge from the path of the magnetic field line. The reflection is caused by changes in the index of refraction due to electron density variations. This acts as a waveguide along the field line (Figure 14).

The ducting effect must occur along much of the length of a magnetic field line for the wave to induce particle precipitation. The ducting effect can only take place if the wave trajectory is roughly parallel to the affected field line. The constraints of ducting along much of the field line, and the trajectory filtering will drastically limit the number of sferics that produce ducted VLF waves in the magnetosphere.

Ducted waves have been observed both from satellites and from the ground. They are frequency dispersed with the lowest frequencies arriving first. When the radio wave is converted to audible tones, the sound is

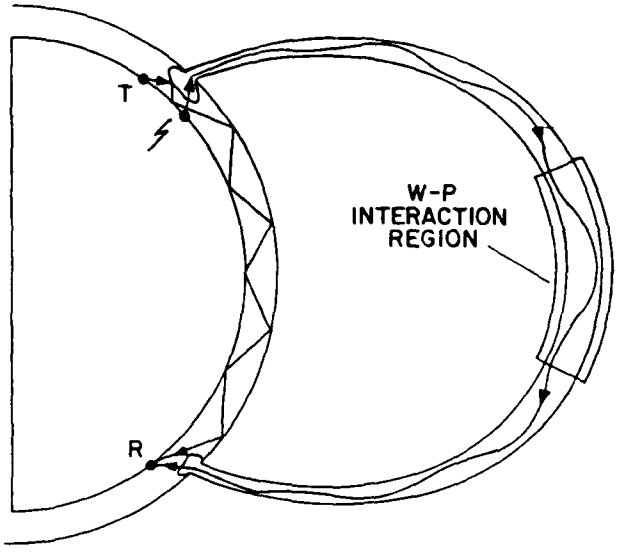

Figure 14. VLF Wave Ducting. The lightning sferic is shown being reflected by the plasmaspheric medium such that the sferic follows the field line, and interacts with the electrons in the magnetospheric equatorial regions. (From Tolstoy et al. 1982)

reminiscent of a whistle. Ducted waves have been dubbed whistlers as a result of this resemblance.

WAVE INDUCED ELECTRON PRECIPITATION

If the duct is stable and allows one or more complete transits, due to reflection from the top of the ionosphere, of the wave from the original hemisphere to the opposite hemisphere, the whistler will interact with the magnetosphere. This interaction is most likely to occur over the equatorial region. Electrons will be precipitated down the magnetic field line towards the direction the whistler is traveling from. The precipitation may pass directly into the ionosphere (direct precipitation) or the electrons may be reflected by the ionosphere and travel back along the field line to be lost in the opposite hemisphere (mirrored precipitation). These two cases are illustrated in Figure 15.

The wave-electron interaction only occurs if both are guided by a magnetic field line. Figure 16 illustrates such an interaction. The electron is gyrating about the magnetic field line. The frequency of the gyration is the electron's gyrofrequency. The electron's velocity is the vector sum of the velocity along the field line and the velocity perpendicular to the field line. The perpendicular velocity is a function of the gyrofrequency.

The electron's pitch angle, α, is determined by the ratio of the perpendicular and the parallel velocities. (Equation 3.1)

$$\tan \alpha = \frac{v_{\perp}}{v_{||}} \qquad 3.1$$

The radio wave has been ducted along the same field line. The maximum frequency of the whistler waves for which ducting between hemispheres will occur is a function of the magnetic field. The electron gyrofrequency is also a function of the magnetic field, and the maximum whistler frequency is one half the minimum gyrofrequency along the field line. The wave particle interaction in question, called cyclotron resonance, can occur only if equation 3.2, the resonance condition, is satisfied.

$$\omega - (\vec{k} \bullet \vec{v}) = \Omega \qquad 3.2$$

Where Ω is the electron gyrofrequency, omega is the whistler frequency (in the VLF range), V is the electron vector velocity, and k is the wave number of the whistler. Equation 3.2 can only be true if there is a significant contribution from the doppler shift term (k•V). This may only take place if the wave and particle are traveling in opposite directions, thus doppler shifting the wave frequency higher in order to match the gyrofrequency. This matching may only take place for a very short time.

The strength of the interaction is determined by the

length of time that the wave and particle are in phase. The particle's pitch angle will be reduced if the particle passes energy to the wave. A particle that receives energy from the wave will be more tightly bound by the geomagnetic field. If a random group of waves acts on a random group of electrons the net effect on the waves will be negligible. Some of the electrons would be more tightly bound by the geomagnetic field, while an equivalent number would see weaker binding. If the initial electron spectrum is isotropic, the result will be to shift the low pitch angle end of the spectrum as seen in Figure 17. The electrons with the lowest pitch angle will be precipitated when electron reaches 100km. A much more likely pitch angle distribution would be heavily concentrated at high pitch angles with a gradual slope towards the lower angles. Much stronger wave particle interaction would be required to move electrons into the loss cone, yielding precipitation once the electron reached 100km, the nominal lower limit on the magnetosphere.

The maximum equatorial pitch angle for precipitating electrons is a function of the ratio of the magnetic field at 100km and the magnetic field at the equator. This is seen in equation 3.3

$$\frac{B_{eq}}{B_m} = \sin^2 \alpha_o \qquad 3.3$$

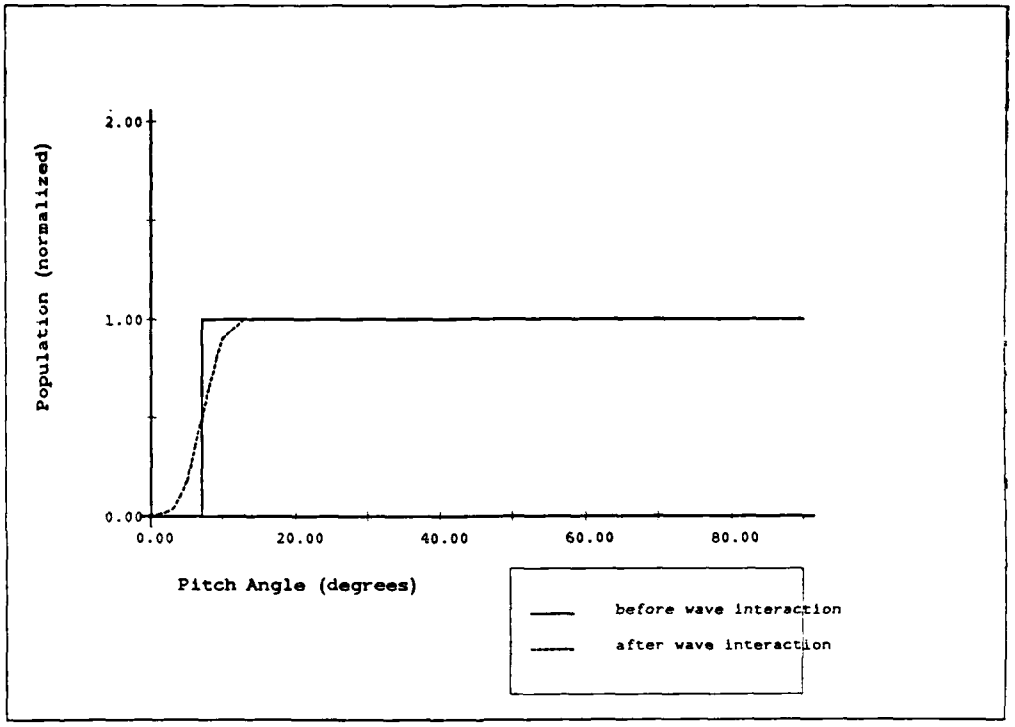

Figure 17. Wave Interaction Effect on Pitch Angle Distribution. The wave interaction may move some of the electrons into the loss cone, seen here as 7 degrees.

Electrons with pitch angles less than α zero will be precipitated, while those with higher pitch angles will turn around at 100km or higher and head towards the opposite hemisphere. Those electrons with pitch angles less than the critical angle will be in the loss cone. The loss cone is found by taking the critical pitch angle and rotating it about the magnetic field line through 360 degrees. Mirrored precipitation occurs for particles whose pitch angles are outside the loss cone for one hemisphere, but are inside the loss cone for the opposite hemisphere. This situation can occur if there are surface magnetic field irregularities at opposite ends of a field line, which give rise to asymmetric values of the field strength at the 100km level in each hemisphere.

THE ELECTRON INTERACTION WITH THE ATMOSPHERE

As the precipitated electrons descend into the ionosphere, they collide with increasingly dense upper atmospheric gasses. Most of the electron's initial energy will ionize or excite the atoms and molecules encountered. Some of the collisions will produce a Bremsstrahlung x-ray [Berger and Seltzer 1972]. The electron is eventually captured in one of the collisions. The x-ray shower from an electron precipitation event will have a much lower energy flux than the electron shower's kinetic energy flux.

The Bremsstrahlung interaction produces photons in all energies below the incident energy. The Bremsstrahlung (braking radiation) x-rays are produced when an electron is decelerated by the electrical attraction of an atomic nucleus. The observed x-ray energy spectrum from a monoenergetic electron shower has a peak just above the minimum energy that can penetrate to the observer's depth. The spectrum gradually tails off towards its high energy limit at the energy of the incident electron beam (Figure 18). The high energy limit is the energy of the incoming electrons. The x-ray spectrum resulting from a range of input energies will have a low energy peak as for the monoenergetic case, but the high energy wing will be a function of the incident energy spectrum. The exponential energy distribution shown in Figure 19 will have a high energy wing that is itself exponential. There still would be no observed photons above the maximum input energy.

The addition of cosmic x-ray sources produces difficulties for electron precipitation detection. The weakest precipitation events will be completely lost in the background. Somewhat more powerful events will show up only as minor enhancements of the background activity. The strongest events will completely overshadow other activity. A more detailed look at the behavior of x-ray bursts is instructive.

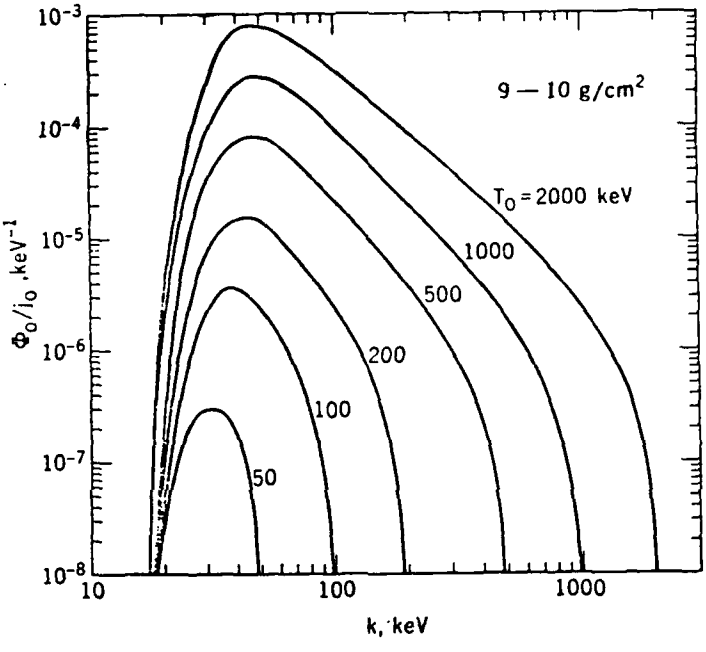

Figure 18. Bremsstrahlung X-Ray Spectra From a Monoenergetic Electron Beam. Range of spectra from monoenergetig beams with energy T_o, as seen with 9-10 g/cm^2 of atmosphere above the detector. (From Berger and Seltzer 1972)

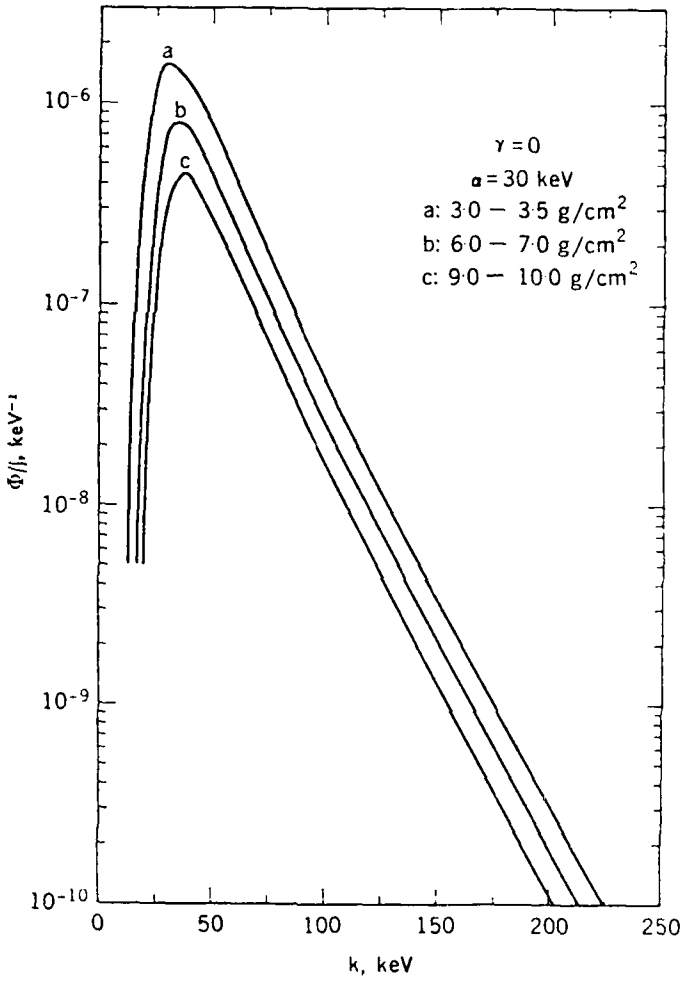

Figure 19. Bremsstrahlung X-Ray Spectrum From an Exponential Electron Distribution. Spectra seen from various depths in the atmosphere, the incident electron spectrum is exponential with an E-folding energy of 30keV. (From Berger and Seltzer 1972)

AN OBSERVED AND MODELED EVENT

Rosenberg et al. (1988) compared data from three hours of a balloon flight from Siple station, Antartica, with a numerical model of wave induced precipitation. The model was parameterized with the known magnetospheric characteristics for the period of the balloon flight, to help quantify the effects of electron density and initial energy on the wave induced particle precipitation process. The observed event was a particularly good example of electron precipitation, and so served as a good event for comparison with the model's results.

Figure 20 is a plot of the x-ray counting rate from one of the balloon flights. The existence of an extraordinary x-ray source is clear. The counting rate frequently jumps by an order of magnitude. A computer algorithm was used to identify 651 microbursts during the three hour period. Each identified microburst was subjectively reviewed to verify its existence.

The microbursts were further broken down into narrow and wide bursts. Figure 21 is a histogram of microburst duration. The tall plateau is distinct from the decaying tail for longer duration bursts. The boundary was subjectively selected to be .6 seconds, the point where the frequency of observations drops off sharply. The frequency of occurrence is largely flat within the narrow

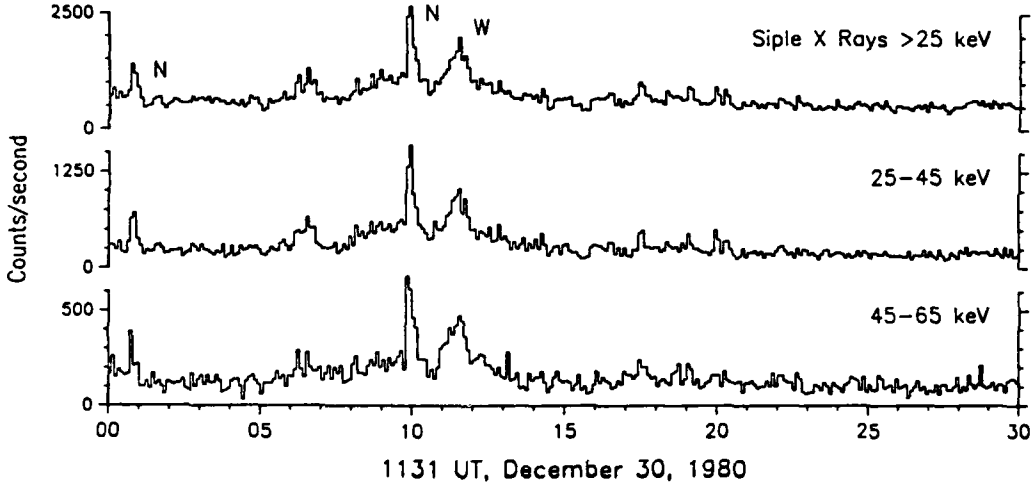

Figure 20. X-ray microbursts seen on balloon data from Siple Station Antarctica. Clear microbursts are seen in the vicinity of 1131 and ten seconds. The integral and first two differential channels are displayed. (From Rosenberg et al. 1988)

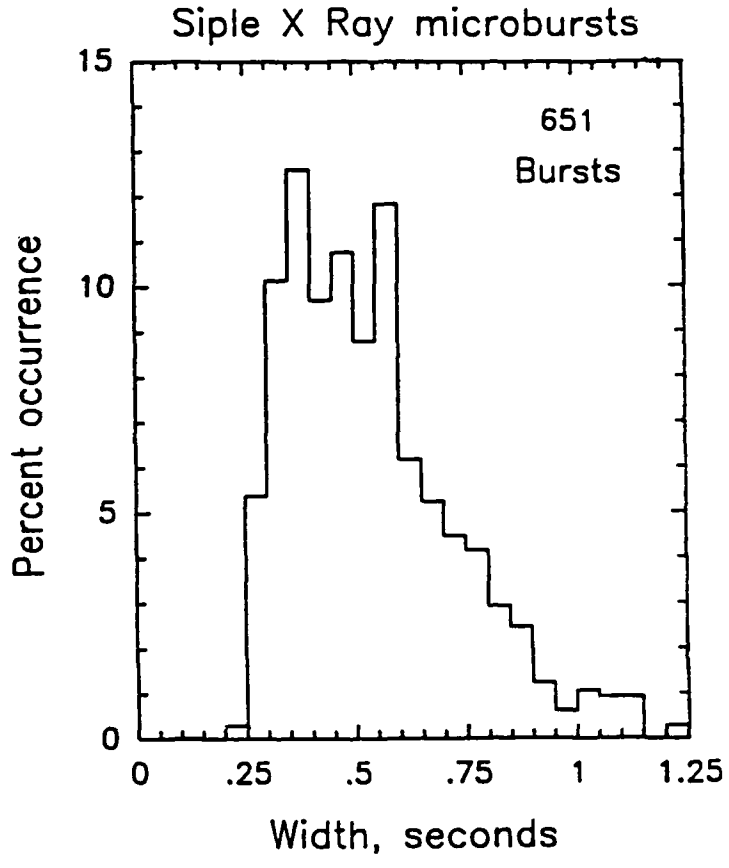

Figure 21. Microburst Duration. 651 microbursts were analyzed and the burst duration was plotted as a function of percent occurrence. 0.6 seconds was subjectively chosen as the division between narrow and wide microbursts, corresponding to direct and mirrored electron precipitation. (From Rosenberg et al. 1988)

bursts. Some finer structure is evident from the two peaks that protrude above the flat plateau.

The spectrum of the wide bursts decays with increasing burst duration, and has no obvious fine detail. The total number of narrow bursts was far higher than the number of wide bursts. The narrow bursts were more than twice as frequent 452 and 199 respectively.

The burst types were composited to develop statistics of each type (Figure 22). Each peak was lined up on the composite peak. As would be expected, the narrow bursts had a much sharper onset and end than the more diffuse wide bursts. Additional information can be gleaned from the peak energy of the two burst types. The narrow bursts had peak energy fluxes twice those of the wide bursts. The narrow bursts were identified with direct precipitation, while the wide bursts were deemed to be mirrored precipitation. The analyzed event can now be used as a test case for the computer simulation.

The observational data was compared to the results of a wave induced particle precipitation model (further developed in Inan 1987). The equatorial electron density and incident electron energy, both factors that affect the k•V, doppler shift, term in equation 3.2, were estimated for the observed phenomena. To be respectively, 20 to 100keV for the incident electron energy, and 10 to 25 electrons per cubic centimeter.

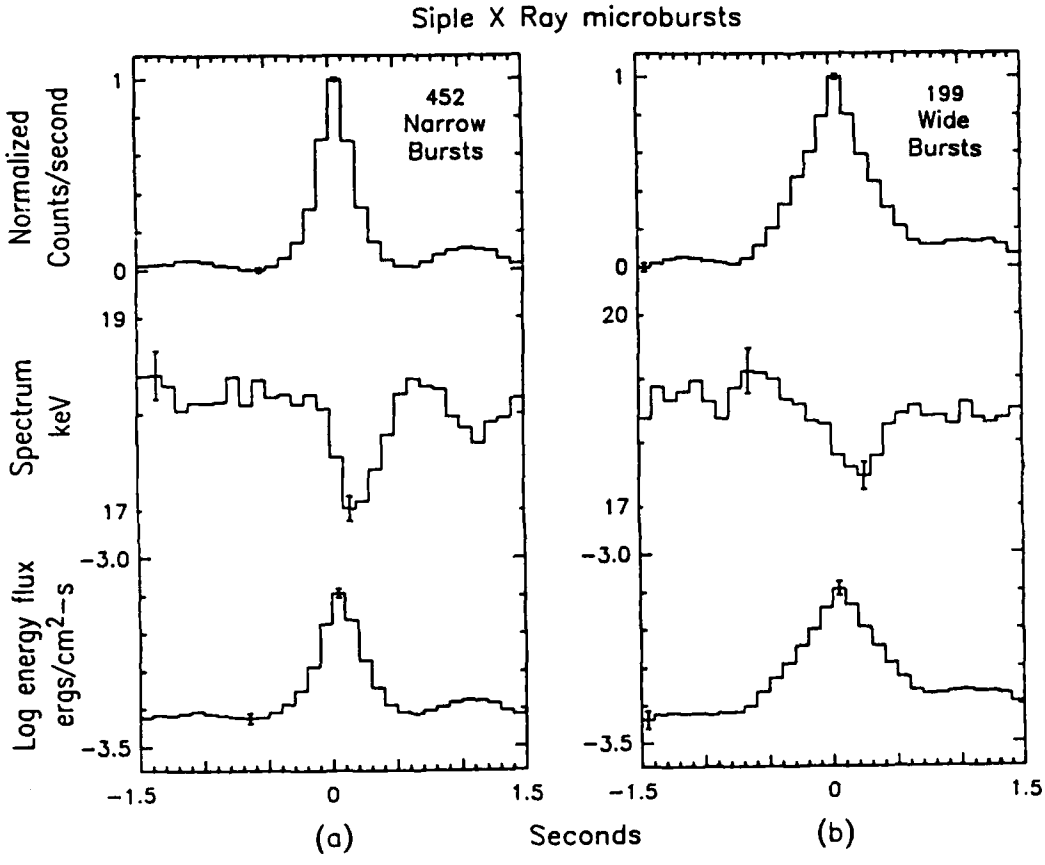

Figure 22. Narrow and Wide Microbursts. The narrow and wide microbursts, using .6 seconds as discussed in Figure 21, are superimposed to develop a statistical picture of the counting rate enhancement, average x-ray energy, and energy flux associated with each type of microburst. (From Rosenberg et al. 1988)

The model used a range of incident electron energy between 25 and 50keV. The range of electron density was between ten and fifty per cubic centimeter. The model produced direct bursts with a duration lasting between .2 and .44 seconds. The mirrored bursts were calculated to last between .4 and .95 seconds. The model's peak energy flux for the direct bursts was twice that for the mirrored bursts (Table 1).

The picture of more frequent and intense direct precipitation versus less frequent and weak mirrored bursts agrees well with the intuitive picture that most of a precipitation pulse passes right into the ionosphere. The mirrored pulse has been reflected off the opposite ionosphere, so some of its electrons will likely have been lost in the opposite hemisphere, and thus have been observed there as direct precipitation. The mirrored pulse travels a much greater distance than direct precipitation, slightly dispersing the electrons in the burst according to energy. Slight variations in kinetic energy, with velocity differences to match, will spread out the pulse along the longer path the mirrored precipitation takes.

There are three phenomena that may be observed in a wave induced electron precipitation burst from a surface VLF source. The VLF wave itself, the ducted whistler wave, and the microburst itself. Direct precipitation

Precipitated electron fluxes (ergs cm^{-2} s^{-1}) and burst durations T(s)

DIRECT (D)

E_o (keV)	N_{eq} = 10 cm^{-3}		N_{eq} = 25 cm^{-3}		N_{eq} = 50 cm^{-3}	
	FLUX	T	FLUX	T	FLUX	T
25	.047	.23	.068	.35	.075	.35
50	.20	.28	.23	.33	.20	.44
100	.66	.23	.50	.30	.51	.38

MIRRORED (M)

E_o (keV)	N_{eq} = 10 cm^{-3}		N_{eq} = 25 cm^{-3}		N_{eq} = 50 cm^{-3}	
	FLUX	T	FLUX	T	FLUX	T
25	.016	.77	.028	.80	.029	.60
50	.09	.65	.10	.60	.09	.95
100	.29	.40	.22	.67	.28	.74

FLUX RATIO, D/M

E_o (keV)	N_{eq} = 10 cm^{-3}	N_{eq} = 25 cm^{-3}	N_{eq} = 50 cm^{-3}
25	2.9	2.4	2.6
50	2.2	2.3	2.2
100	2.3	2.3	1.8

Table 1 (From Rosenberg et al., 1987)

should be easier to observe than mirrored precipitation due to the fact that the direct precipitation is falling into the same hemisphere that the VLF wave originated from. The source should be more easily identified, as it is located in the same hemisphere as the observer. Direct precipitation may be caused by the first hop of the whistler. The whistler will probably be at its maximum strength, as the duct stability will not limit this first pulse. Conversely, the whistler that produced the precipitation will be hard to identify, as it would have to return on a second hop to be identified with its precipitation burst. The VLF wave source and the direct precipitation pulse can be correlated easily, but the whistler can only be identified by measurements from both hemispheres, or if the whistler returns to the hemisphere it originated from.

An observation of mirrored precipitation will be due to either a whistler that started in the observer's hemisphere and is on a return hop, or a whistler with an origin in the opposite hemisphere. The stability of the duct affects the returning whistlers, while the source of the opposite hemisphere whistlers are harder to identify. It will generally be easier to correlate the whistler with the precipitation for mirrored precipitation. It will be difficult for both the mirrored and direct cases to correlate the precipitation with both the whistler that

caused it, and the source of the whistler.

Another indicator of dispersion of the pulse is the time-dependent spectral characteristics of the bursts. This is particularly clear in Figure 22. The bursts showed up first at higher energies and gradually lost individual x-ray energy while the net energy flux increased. The average burst x-ray photon was actually less energetic than the average background emissions.

TRANSMITTER WHISTLER SOURCES

Even though, lightning is far and away the most powerful terrestrial radio source, there are man-made transmitters whose frequencies have been chosen to maximize the carrying distance by using the earth's atmospheric waveguide to the greatest extent possible. Although the purpose of the transmitters is for radio navigation, they have been used to monitor the ionosphere along the path length to the receiver [Carpenter and Inan 1987, Inan and Carpenter 1987, Tolstoy et al. 1986]. The transmitter frequencies have been chosen to be transmitted well by the Earth Ionosphere waveguide.

Sudden perturbations of phase and amplitude have been correlated with whistlers. These changes have been attributed to electron precipitation increasing the ionization along the radio path (Figure 23).

This makes the received signal an excellent

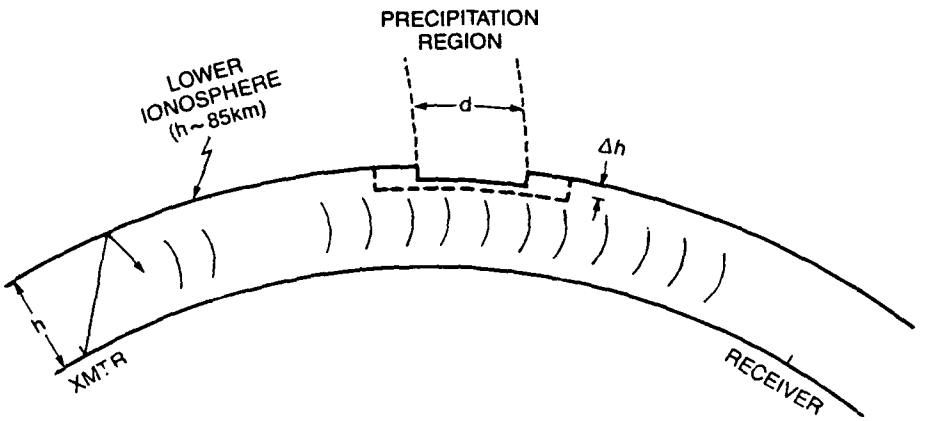

Figure 23. Earth Ionosphere Waveguide Changes due to Electron Precipitation (From Carpenter and Inan, 1987)

diagnostic of the ionosphere, since perturbations of the ionosphere are the major effect on the signals (Figure 24). Another implication of these transmitters is as whistler sources. A continuously transmitting source will produce continuous waves in the magnetosphere. If these waves cause electron precipitation, the precipitation will be steady and not detectable as separate from the cosmic ray background. If the transmitter is modulated to produce square waves, it should be possible to detect the onset of the precipitation from each pulse.

SUMMARY

Wave induced particle precipation has three basic requirements. The first requirement is the availibility of VLF radio waves. In the mid-latitudes, these waves may be either lightning sferics or powerful VLF/ELF radio transmitters. The powerful lightning sferics are readily available on a global basis, as it is relatively rare to find a period when there is no convection anywhere in a large region of both the Northern and Southern Hemispheres. Thunderstorms are, however, unpredictable at a given place and time. The transmitter waves are much less powerful but may be controlled. Continuous monitoring for electron precipitation is perfectly justifiable as whistler sources are routinely available.

The second requirement is ducting. Ducting is only

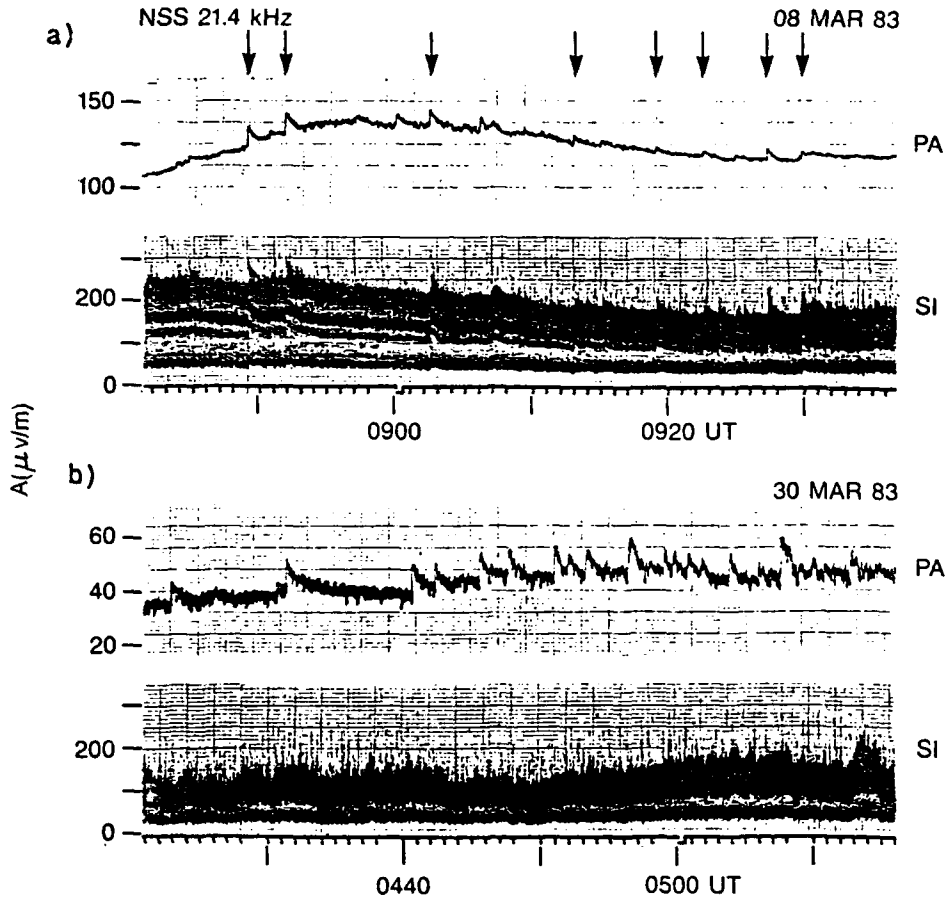

Figure 24. Sudden Amplitude Changes Associated with Whistlers. The sudden amplitude changes seen on VLF receivers at Palmer (PA) and Siple (SI) research stations in Antarctica. (From Carpenter and Inan, 1987)

detectable by the presence of whistlers, and ducting is unpredictable since it is a function of the state of the magnetosphere. Nonetheless, observations often reveal the presence of whistlers.

The third requirement is electrons available for precipitation with pitch angles near the loss cone. The electron density increases in association with the magnetospheric contraction associated with substorms [Hargreaves 1979] and is relatively high for several days as the substorm subsides. Various electronloss mechanisms will be most efficient during this period, including wave-particle interactions.

The whole wave-particle interaction is pyramidal in nature. Numerous VLF waves are constantly being transmitted, and most waves leak into the magnetosphere. Enough waves are ducted for whistlers not to be uncommon, but electron precipitation is uncommon.

CHAPTER 4

THE WAVE INDUCED PARTICLE PRECIPITATION CAMPAIGN

INSTRUMENTATION

The Wave-Induced Particle Precipitation (WIPP) Campaign was a coordinated effort funded by the National Science Foundation with support provided by NASA's National Scientific Balloon Facility and Goddard Space Flight Center's Wallops Island Flight Facility. The campaign involved researchers from Lockheed Corporation, Stanford, Cornell, and the Universities of New Hampshire(UNH), Maryland(UMCP), and Washington(UW).

The campaign ran between 15 July and 1 August 1987. Wave particle precipitation had been observed within the plasmasphere only with VLF recievers [Carpenter and Inan 1987] and a rocket flight [Goldberg et al. 1987]. The campaign was based at Wallops Island, whose magnetic fieldlines are well within the plasmasphere, with a wide variety of local instruments. The goal was to view a precipitation event overhead with simultaneous measurements

The campaign attempted to detect electron precipitation from both lightning and transmitter sources within the plasmasphere. The Wallops Island Flight

Facility was tied into the State University of New York (SUNY) at Albany East Coast Lightning Detection Network. This network was used to monitor the production of lightning within 300 miles of Wallops Island. The transmitter part of the experiment was supplied by modulating the U.S. Navy 21.4kHz (NSS) transmitter at Annapolis. The modulation took place between 0500 and 0515Z and between 0815 and 0830Z each night. The transmissions were altered to a square wave with a five second period, three seconds on, and two off. This might cause precipitation with the characteristic five second period.

The intent of the campaign was to deploy a wide array of instrumentation and make simultaneous observations. The instruments were rocket- and balloon-borne as well as ground-based. The ground-based instruments consisted of a photometer (Lockheed), a micropulsation magnetometer (UNH), VLF receivers (Stanford), and a riometer (Relative Ionospheric Opacity Meter) (UMCP). An additional photometer (UW) and an x-ray detector (UMCP) were carried aloft by each of four balloons. The rocket carried particle detectors (UNH), an imaging photometer, and VLF wave receivers (Cornell).

The riometer monitors ionospheric absorption of background radio transmissions. A sudden burst of ionization in response to electron precipitation can be

seen as an increase in cosmic radio absorption with a gradual return to the background radio noise as the ionization levels return to normal. The riometer views the ionosphere overhead, detecting local electron precipitation.

The VLF receivers monitor the signal from U.S. Navy VLF transmitters. If precipitation along the path to the receiver changes the local Earth ionosphere waveguide characteristics, these changes will cause phase or amplitude shifts of the signal recieved. The advantage of the VLF receivers is that they monitor the entire path length along the earth's surface between the transmitter and the reciever. The disadvantage of the VLF receiver is that electron precipitation is equally detected along the path length without any information about the location of the electron precipitation.

The micropulsation magnetometer detects local changes in the magnetic field due to the electron precipitation current. Like the riometer, the micropulse magnetometer has a limited range of detection.

The photometers detect photons given off during the recombination of ions. A sudden increase of this light will be due to a sudden increase in the ionization levels, presumably caused by electron precipitation. Photometers have a localized view of the overhead ionosphere and must have filters to pick out the emission lines from the

recombining atoms.

X-ray detectors are also local detectors, but they detect secondary effects from the precipitation; namely Bremsstrahlung x-rays. One problem with the x-ray detectors is the atmospheric absorption at lower levels. Any surface measurements will be dominated by emissions from the Earth. Once above the surface, cosmic ray emissions will dominate. Cosmic ray particles penetrate deeper into the atmosphere than wave-induced precipitation. There will be a maximum of x-rays produced by cosmic rays between 20 and 30km above the earth's surface. Measurements of x-rays produced by the precipitating electrons will have to be made above the level to which the cosmic rays penetrate.

The particle detectors measure the precipitation directly, giving detailed information about the actual electron spectrum. The rocket borne particle detectors also reach much greater altitudes. This greater height puts much less absorbing material in the path of the incoming electrons. The lower absorption allows higher time resolution due to a higher signal. The high time resolution is required for the rocket flights as the total flight time is limited to approximately 10 minutes.

SCIENTIFIC CONSIDERATIONS

Wallops Island was a convenient location for basing

the experiment. NASA was able to provide substantial support from the existing Flight Facility. The observations had to be made from middle to low latitudes in order to observe whistler-related electron precipitation caused by lightning sferics or modulated transmitter waves. Outside the plasmapause and in the auroral zone, conditions are better for observing other phenomena whose origin is magnetospheric perturbations or the solar wind. Any effects whose origins are outside the plasmapause will be damped out at the plasmapause, since Wallops Island lies on a magnetic L-shell of less than 2.75.

Collocating the instruments had some disadvantages. The riometer and VLF receivers were more sensitive to direct sferics than to the absorption due to the precipitation. If the thunderstorm is close, yielding the highest chance of local electron precipitation, observing the effects becomes more difficult. This due to the instruments whose data is contaminated by the strong sferic signal.

The Wave Induced Particle Precipitation Campaign consisted of an array of tested methods for observing particle precipitation. Many of them have been used at high latitudes to detect particle precipitation in conjunction with observed whistlers with sources other than lightning. These include the riometer, x-ray

detector [Rosenberg et al. 1988], and photometer.

There is a wide variety of energy sources for high latitude whistler made waves. Aurora generated waves and VLF chorus emissions originate within the magnetosphere. The magnetospheric generation of the waves implies no absorption transiting to the magnetosphere. These high latitude measurements showed wave-induced precipitation due to waves with different sources from those under consideration here [Rosenberg et al.1988, Gaines et al. 1986, Rosenberg and Dudeny 1986, Lanzerotti and Park 1978].

Lightning and transmitter-induced precipitation occur most easily at low latitudes, within the plasmasphere. The higher electron density will yield more electrons to be precipitated. Auroral and substorm-related precipitation will be effectively barred from the plasmasphere by the plasmapause. The methods of observing particle precipitation will be applicable independent of the nature of the source or the geographical region observed.

The small spatial scale of the midlatitude precipitation events creates problems for instruments with a local field of view. Midlatitude precipitation has primarily been observed through monitored VLF transmissions displaying Trimpi Events, sudden phase and/or amplitude shifts with gradual return to

predisturbed values (Figure 24). The monitored transmissions may travel along several thousand miles of the Earth Ionosphere Waveguide, producing a detector area a thousand times that of the instruments that monitor the local ionosphere for overhead particle precipitation.

The goal of the local instruments was to detect wave-induced particle precipitation from a variety of simultaneous measurements. A single, clearly identifiable precipitation event would make the entire effort a success. The available measurements would allow observation of changes in ionization level (riometer, and ground and balloon photometers), Bremsstrahlung x-ray production (balloon x-ray detector), and magnetic perturbations (micropulsation magnetometer). No previous event had been analyzed with the thoroughness the WIPP instruments allowed.

PRACTICAL CONSIDERATIONS

The very size and scope of the campaign was something of a drawback. The cost of maintaining such a large body of scientists and support personnel limited the duration of the experiment. The six-week program originally proposed was pared down to two weeks. The campaign had four balloons and one rocket to launch during this two week period. During these two weeks, the proper combination of available waves, magnetospheric ducting,

and enhanced equatorial electron density was required to produce one local precipitation event.

The magnetospheric ducting and enhanced electron density occur in a disturbed magnetosphere, which generally follows the injection of additional electrons by a magnetospheric substorm. Weak waves are continously available during modulation of transmitter sources but the strong lightning sferics are somewhat less common.

The much stronger lightning sferics are most common during the Wallops Island summer. The most common time of occurrence is in the late afternoon (Wallace and Hobbs 1977). Thunderstorms can be expected to occur on roughly one in three days.

The afternoon thunderstorm maximum conflicts with observing small changes in the ionosphere, as the ionization levels of the daytime ionosphere are highly elevated (Figure 25). Any ionization produced by particle precipitation must be observed against a much higher background, effectively masking the precipitation event. The balloon float level also lies below the ionosphere and has the further disadvantage that the float altitude is not stable when the stratosphere cools after sunset.

The daylight hours thus ruled out use of the ground-based or balloon-borne tools to indicate particle precipitation. This rules out the possibility of a daytime rocket launch, since the rocket is limited to 10

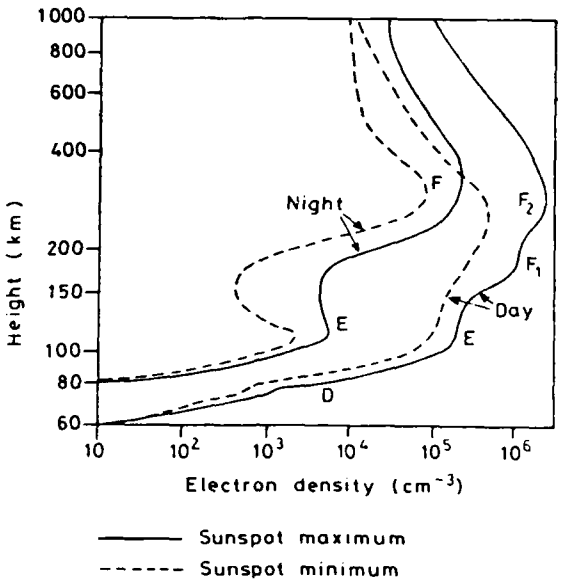

Figure 25. Diurnal Changes to the Ionosphere. The D, E, and F regions are shown for sunspot maxima and minima (From Hargreaves, *The Upper Atmosphere and Solar Terrestrial Relations*)

minutes of data, and it would not make sense to launch the rocket without the hope of a previous indication of precipitation or supporting ground measurements. The entire campaign was conducted during the nighttime hours. Thunderstorms did take place on several nights during the campaign, and provided ample lightning as will be seen in the results (chapter 6).

The Wave Induced Particle Precipitation campaign was a coordinated attempt to study a problem from a wide variety of methods. The limited duration due to the scope of the effort, and the inherent instrument liabilities combined to make the campaign a high risk proposition with a correspondingly high payoff in the event of a positive result.

CHAPTER 5

THE UNIVERSITY OF MARYLAND PORTION OF THE WIPP EXPERIMENT

THE X-RAY DETECTOR

The University of Maryland effort was a dual one, with the ground-based riometer and four balloon-borne x-ray detectors. The NSBF provided four three million cubic foot helium balloons and the required telemetry packages. The balloons reached a nominal altitude of 38km.

The x-ray detectors were flat, 12.5cm diameter NaI crystals (Figure 26). Counting rates were sampled every ten milliseconds for each of the six differential channels and the integral channel. The tube size was chosen to be large to increase the counting rate statistics. This would make the detection of a relatively weak event more likely.

The differential channels allow detailed investigation of any detected x-ray burst (Table 2). Spectra from the differential channels could be compared with previous measurements, particularly to see whether they "softened" during the burst as has been previously observed in Rosenberg et al. [1988].

The time resolution was high enough to study the

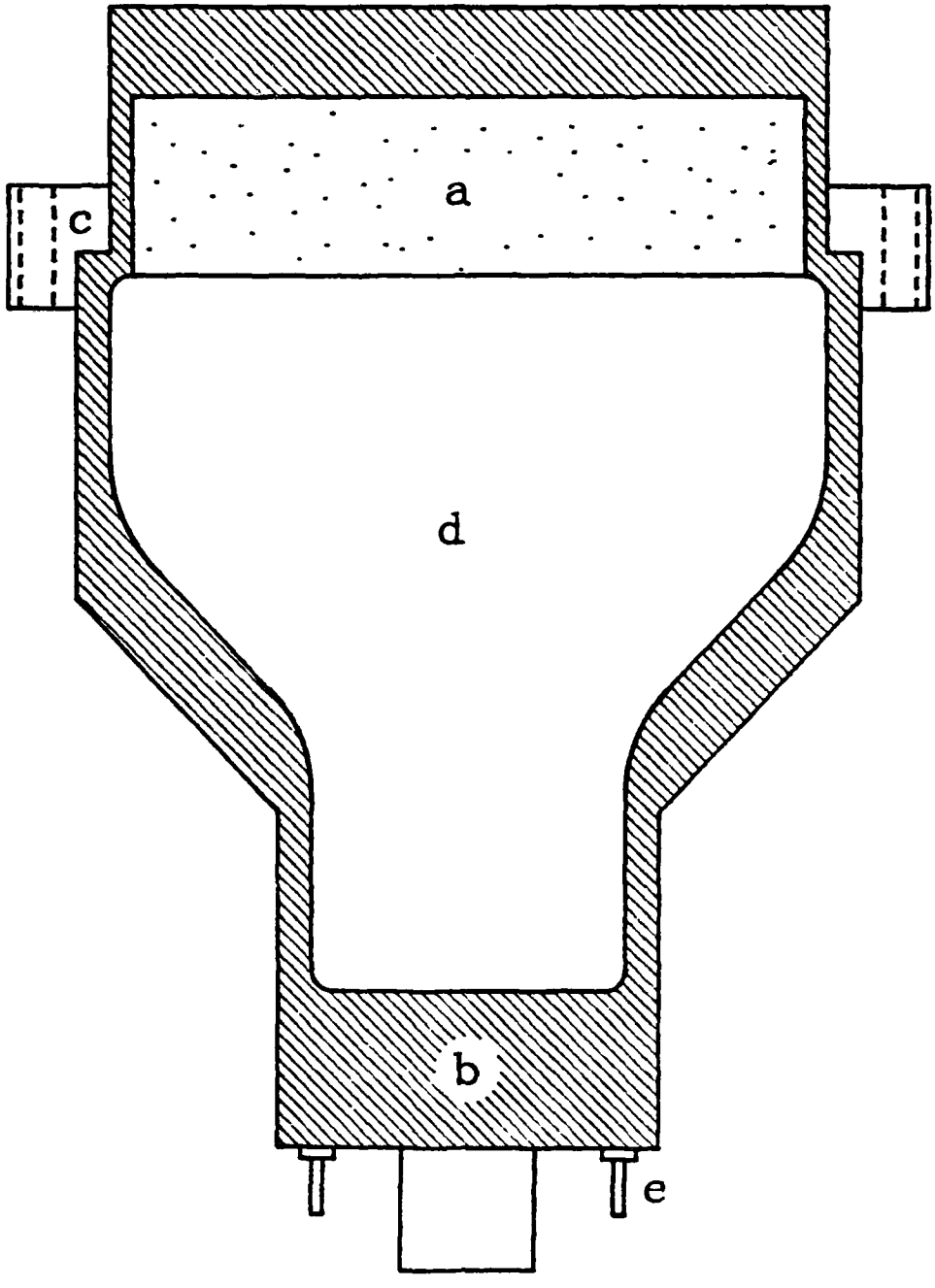

Figure 26. The X-Ray Detector. (a) NaI crystal; (b) silicon compound sealer; (c) rim with mounting holes; (d) tube chamber; (e) output leads. [Drawing by Ron Berg]

Table 2. X-Ray Detector Differential Channels

Channel	Energy Range (keV)
1	15-25
2	25-35
3	35-50
4	50-75
5	75-100
6	100-125
7	125-175
8	>175

time-dependent behavior of individual microbursts. The WIPP balloon results could be compared with the Antarctica balloon data from Rosenberg et al. (1988). The detailed behavior of wave-induced particle precipitation whose sources were magnetospheric VLF chorus waves and lightning sferics could be compared to determine both the similarities due to common controlling physics as well as the differences due to different wave sources and magnetospheric electron source regions.

The conditions that the payloads would operate under were quite extreme. The temperature and pressure at 38km would be around -20°C and 3 millibars (U.S. Standard Atmosphere). The balloon would pass through much colder temperatures, -50°C would not be surprising. As the summer tropopause is quite high and cold, even -80°C is not an uncommon value from the author's experience with radiosonde data. The balloon would pass through the upper troposphere and lower stratosphere fairly quickly, so each payload was insulated against the extreme cold by a two-inch-thick box of styrofoam. The insulation and the heat generated by the electrical circuits kept the payload temperatures above freezing (Figure 27).

The x-ray detector tubes (Figure 26) had twelve hundred volts across the base leads. The current was supplied by nickel-cadmium batteries, and the voltage was stepped up by power supply circuits. These power supplies

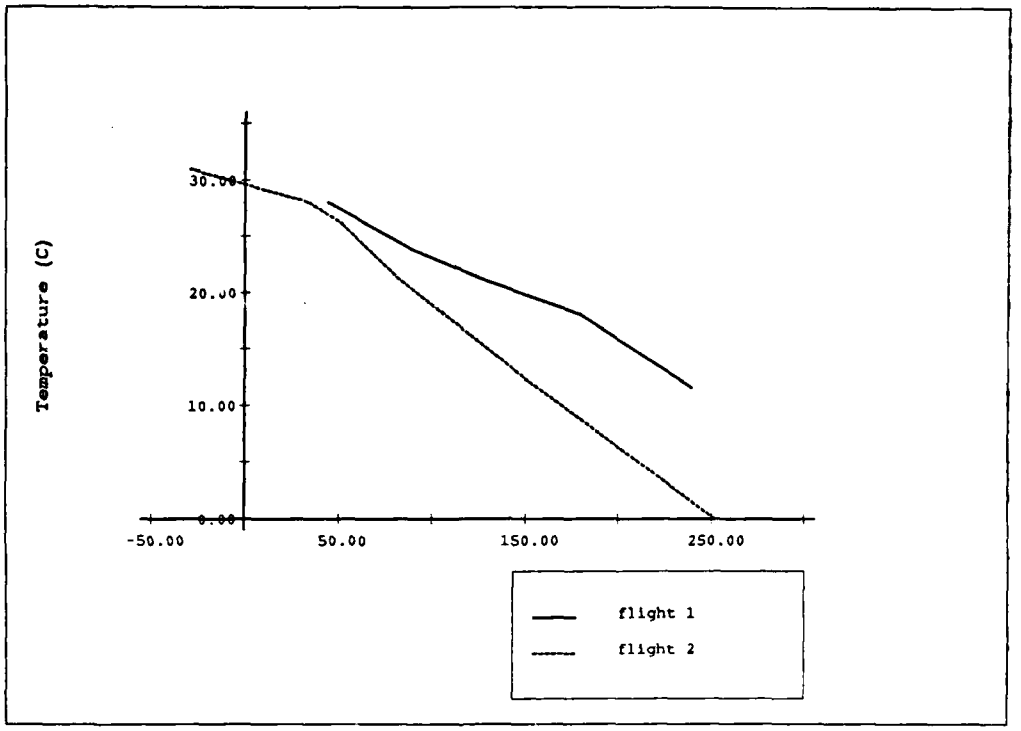

Figure 27. Temperature Trace for Balloon Flights 1 and 2. Internal payload temperature is plotted against time after launch.

were tested for stability of output for varying input, and were found to be quite stable for a relatively wide range of inputs (Figure 28).

The low pressure was more of a design problem than the cold. The 1200V is quite sufficient to arc the short distances across the base of the tube even for higher pressures than would be observed at float level. The power supply and base of each of the four detectors were placed in a silicon compound to combat arcing. The compound was poured in two phases. The first pouring covered from the base of the power supply to just below the connection to the x-ray tube. The poured silicon was placed in a vacuum chamber at 5mb for ten minutes to eliminate any air bubbles introduced into the mixture when it was stirred.

The tubes were then connected and the combination tested to ensure the continued operation of the power supplies. The pouring and vacuum chamber process was repeated to seal the tubes to the power supplies.

The fully sealed tubes were again tested by placing each in the vacuum chamber for twenty four hours. The initial pressure was pumped down to 2mb, and enough air leaked in for the final pressure to be roughly 12mb after the full day. The background count rate was used to monitor the tube performance and remained stable for each case.

The sealed tube was also checked to make sure that the

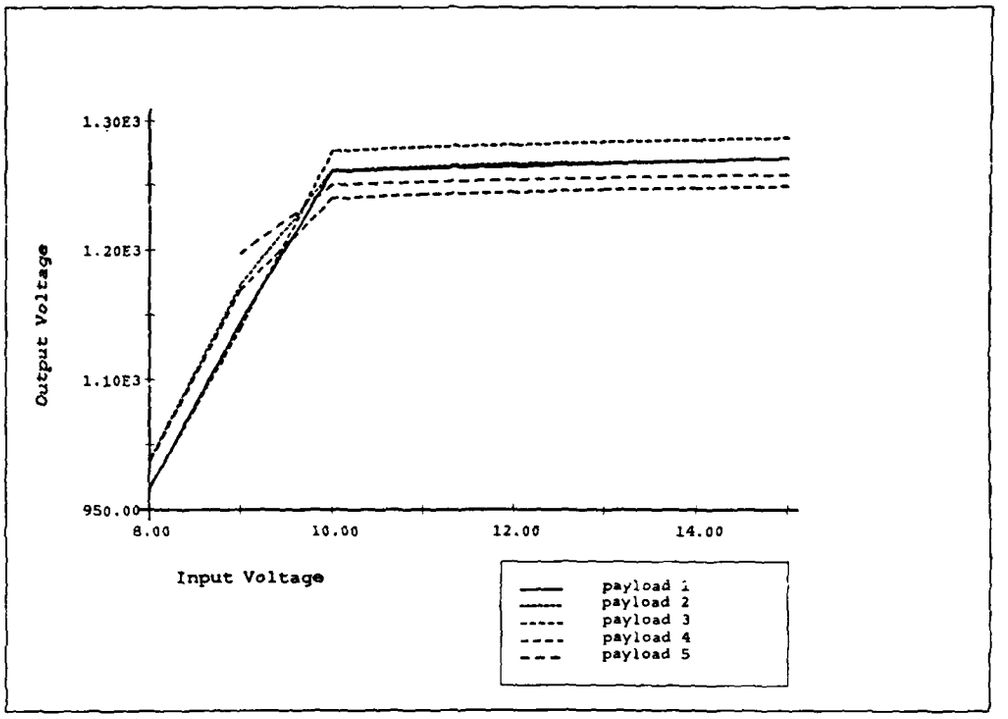

Figure 28. Power Supply Output Stability. All power supplies were stable for voltages 10V.

output was proportional to the input energy (Figure 29). The 22keV and 88keV x-ray emission lines of CD 109 were used to test the proportionality. The magnitude of the outputs varies from tube to tube, but all had proportional output.

The rest of each payload was assembled. The complete payload was now subjected to a combined temperature and pressure test. The temperature was lowered from room temperature to -50°C at a rate of 10°C an hour (Manufacturer's specifications). Intermediate measurements of the background count rate for each of the channels monitored the performance of the payload. Figure 30 is a plot of the 35-50keV channel for each tube. The payloads performed well above 0°C, as differences in the room temperature output were accounted for within the circuit boards at a later stage. All of the payloads showed significant difficulties at temperatures below -20°C, and this was well documented in the design specifications. The tube design was such that efficiency fell steeply after -20°C.

The pressure was lowered once the temperature was -50°C. The minimum pressure was only 27mb for a stable -50°C, since the payload generated enough heat to warm the rarified air faster than the chamber could cool it. Payload #1 performed well. The signal from payload #2 dropped out while the pressure was being reduced. Signal

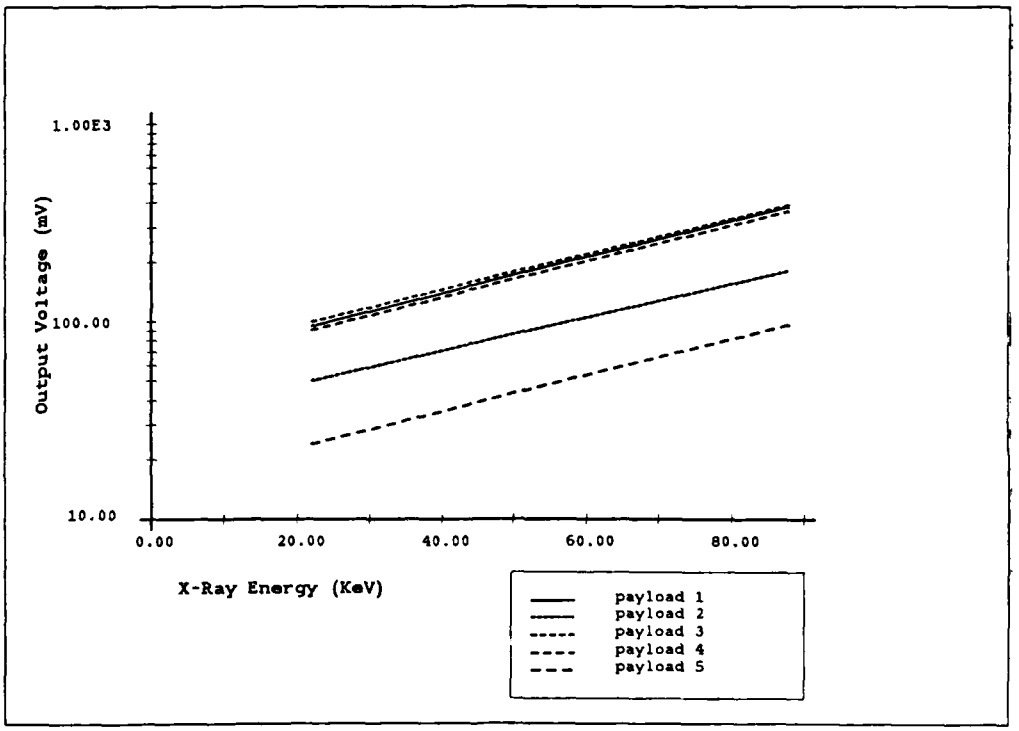

Figure 29. Sealed Tube Check with a CD 109 X-Ray Source. The proportionality of output was tested for each payload for Cadmium 109 22keV and 88keV lines.

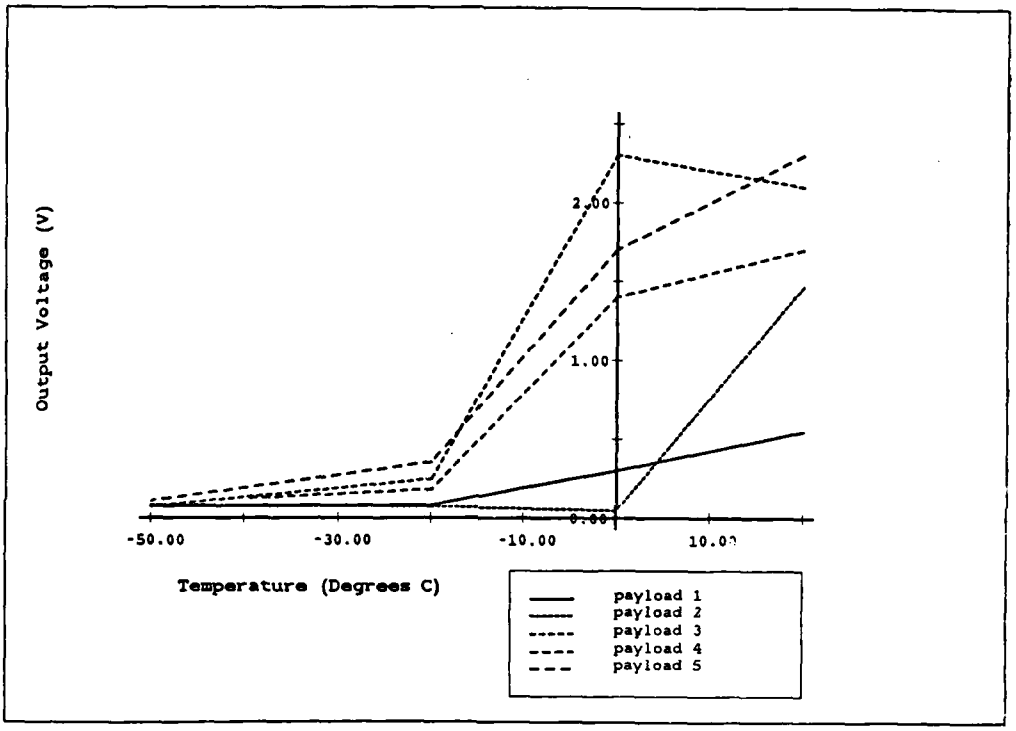

Figure 30. Temperature Test of Assembled Payloads. Payload performance fell off between 0°C.

loss pointed to arcing within the tube/power supply system and payload #2 was designated the spare. Payload #3 was only subjected to 27mb at -10°C. Further combined testing was suspended due to the failure of payload #2, and the fact it would be unlikely for the temperature inside the payload to drop well below 0°C.

Despite the careful testing, arcing problems occurred during flights 3 and 4, payloads #5 and #4 respectively. Post-flight testing indicates that the base of the tube was not properly sealed at the factory. Repeated failures have occurred in tubes from payloads #2, #4, and #5. No arcing has been detected in post-flight testing of the two tubes that passed the combined test and did not fail in flight. (payloads #1 and #3)

BALLOON LAUNCH CONDITIONS

The payloads were assembled and tested. Criteria had to be determined for the actual launch of the balloons. The first consideration was a stable float altitude. The balloon could not be permitted to reach float altitude before sunset. If float altitude was reached while the sun was still shining on the semitransparent balloon material, ballast would be prematurely dropped to maintain a steady altitude for the daylight period. Then balloon would cool off more quickly than the stratosphere after sunset and fall due to its reduced bouyancy. A target launch time of

roughly 2300Z was chosen since ascent was estimated to take two hours and local sunset at the float altitude would be around 0100Z.

The transmitter portion of the experiment was active every night. The Annapolis (NSS) 21.4kHZ transmitter was modulated on a on a .2Hz cycle between 0500Z and 0515Z, and 0815Z and 0830Z. A 2300Z launch time, two hour ascent, and a minimal four-and-a-half-hours at float altitude would provide data from at least the first transmitter period. An eight hour flight was not considered out of the question, and would catch both transmitter episodes. Some transmitter data would be available for almost any launch time, and the transmitter portion of the experiment did not affect the launch decisions.

The minimum lag time between a launch decision and a balloon's arrival at float altitude was four hours. The probable maximum duration of an individual set of events would be three hours, using as an example the extraordinarily intense bursts observed on one of Rosenberg et al.'s balloon flights. Each of the seven Rosenberg et al. (1988) flights was in the air for over twenty four hours. The longest set of bursts was three hours. Consequently, observed precipitation could not used as the criterion for launch.

The ground-based data was monitored each night for signs of electron precipitation. A precipitation event

would be indicative of magnetospheric conditions favoring further electron precipitation. The difficulty of this was the short duration of the late July night. The ionosphere took some time after sunset to quiet down enough for useful measurements. Even if precipitation was visible immediately, it would be after midnight before the balloon was gathering data at float altitude. The maximum flight time remaining would be four hours. Continued delay brought diminishing flight time.

The magnetospheric conditions that produce electron precipitation are not easily forecast. The only predictor would be a previous magnetospheric substorm; these are also relatively rare and not well forecast. The balloon launch decision had to be anticipatory due to the lag between the decision and the commencement of useful data.

The potential for thunderstorms is easier to forecast. A thunderstorm in the general area was all that was needed since the sferics are so well transmitted by the Earth Ionosphere Waveguide. The thunderstorm forecast became the main launch criterion. This was somewhat by default, since the more critical factors, namely the potential for magnetospheric ducting and an enhanced equatorial electron density, are not observable except with particle precipitation measurements.

THE BALLOON FLIGHTS

Wallops Island was under a very dry high pressure ridge for the first week of the experiment, between July 15 and 24, 1987. No thunderstorms occurred until the airmass was modified by moisture off of the Atlantic Ocean. Unforecast thunderstorms occurred late during the evening of July 24. The first thunderstorm forecast was for the evening of 26 July. The decision was made to launch before the arrival of the area of thunderstorms. The size of the balloon (three million cubic feet) was such that the maximum wind speed for a safe launch was eight knots. The wind had to remain under eight knots for the fourty-five-minute period between the start of inflation and launch.

Stable winds could not be expected during a thunderstorm, and the balloon had to be launched at 2207Z. This was almost an hour earlier than the strict requirements for a stable float would have dictated. Lightning was visible when the balloon was launched, thus delay was unsafe to the launch personnel, and the balloon could not be retrieved once inflation started. The balloon reached float before sundown, and gathered only four hours of data before descending.

The second balloon flight took place the next night. An area of strong thunderstorms was developing northwest of Washington, D.C. This area moved over Wallops Island

around 0600Z. The balloon launch was at 0020Z and was uneventful. The problem for this flight was strong stratospheric winds, approximately 36 m/s. The average for summer over Wallops Island would be around 25 m/s[Wallace and Hobbs 1977].

The strong stratospheric winds rapidly pushed the balloons to the edge of the Wallops' radar range. The combined payload and telemetry packages weighed over two hundred pounds and posed a substantial hazard to aircraft in the unlikely event of a collision on the balloon's downward path. The FAA (Federal Aviation Administration) required that the balloon come down before it left the Wallops radar range. As noted above, the x-ray detectors failed for balloon flights #3 and #4, so descriptions of those flights are not needed.

SUMMARY

The balloon flights were hampered by payload failure and short duration. The effective data was reduced to a quarter of what was hoped for. The riometer was operational throughout the experiment but had problems with contamination due to lightning as outlined in chapter 4.

CHAPTER 6

RESULTS OF THE EXPERIMENT

PRELIMINARY INDICATIONS

All of the experimental data was screened during the experiment. The balloon data were continuously monitored throughout each flight. The ground based instruments (including the riometer) were monitored during each balloon flight, and any time the rocket was ready to launch. After the first week the rocket counted down every night and held at a count of ten minutes to launch. The rocket was waiting for ground based indications of particle precipitation, so the raw data were closely monitored.

The data were further inspected each morning for signs of precipitation after the investigators had left. The consensus opinion pointed to two periods of Trimpi events on the VLF receivers, the first taking place twenty minutes after the termination of the second balloon flight. The second period of events was during the rocket flight.

There were some indications of very slight activity during the last hour of the second flight. These were

weak enough to be tagged merely as events that should be investigated particularly carefully.

The data that were examined as part of this study included part of the riometer data, and the whole of balloon flights one and two. The last two flights were too heavily contaminated by arcing within the detector to place any trust in the data.

THE RIOMETER

The riometer data available for examination was somewhat limited. The available data was screened for periods contaminated by noise due to thunderstorm sferics. The quieter periods were analyzed to determine the power spectrum of each transmitter period. The modulation of the transmitters would theoretically yield precipitation with the same period as the modulation, five seconds.

The periods that seemed to have a peak at .2Hz were plotted in one minute segments and closely examined for the Trimpi signature of rapid increase of absorption, followed by gradual return to normal. Failing such obvious signs, the segments were inspected to determine whether the peak detected in the spectrum was due to increased absorption of the background, or random fluctuations. An example is shown in Figure 31 of one spectrum that showed a strong peak around .2Hz. The plot of the raw data is Figure 32, and the smoothed plot for

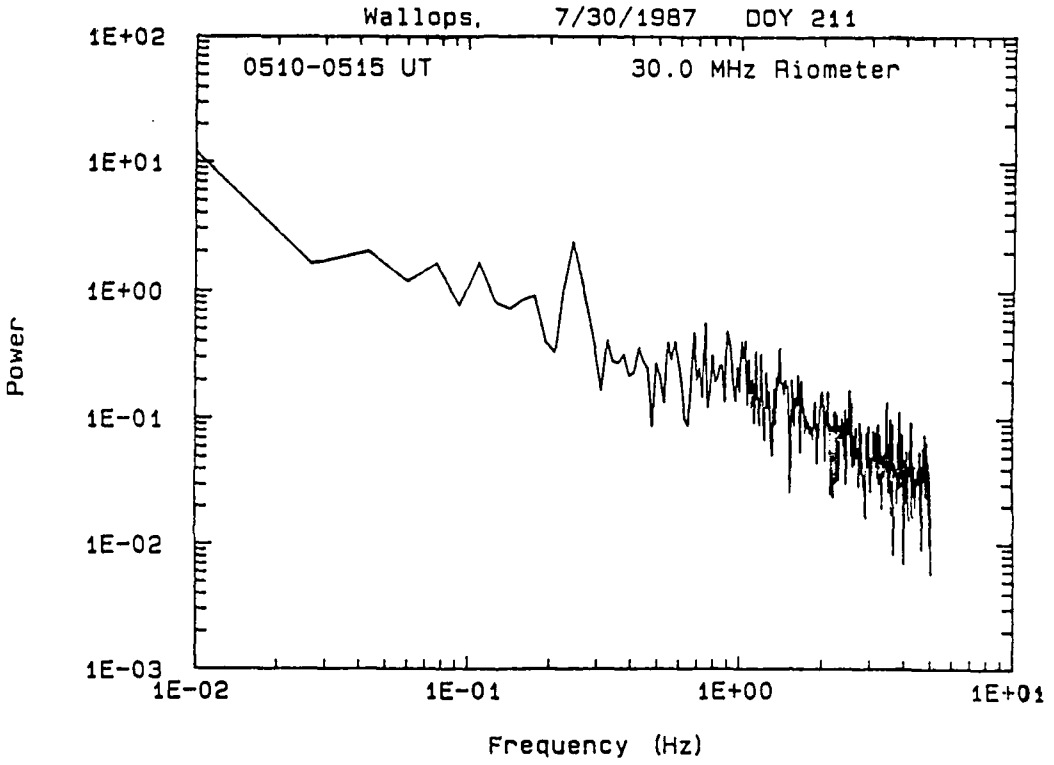

Figure 31. Riometer Spectrum showing a good peak at .2Hz.

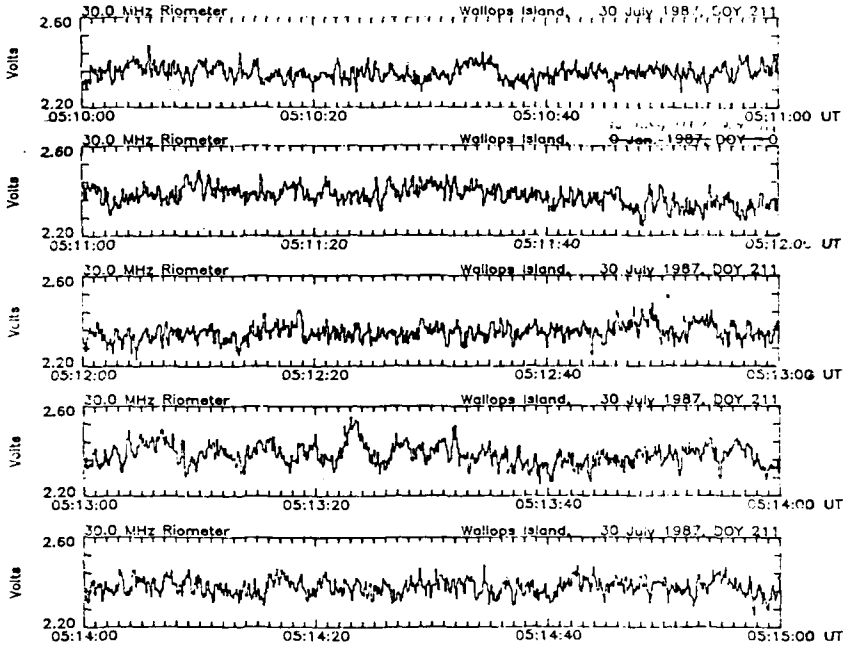

Figure 32. Plot of 5 minute voltages for the period used in Figure 31.

this period is seen in Figure 33. None of the spectra showed signs of transmitter-modulated precipitation.

The riometer data recorded during the two usable balloon flights was also examined in depth. The data corresponding to the first flight was somewhat contaminated by lightning sferics, but was still usable. Flight one's riometer data did not have any evidence of increased absorption events.

The second flight riometer data was uninteresting for the first portion of the flight, but became a lightning detector for the last forty-five minutes of the flight. The strong noise peaks correlated quite well with the positive strokes observed on the SUNY Albany lightning detection system. The frequent, strong bursts eventually saturated the riometer. The saturation hides any information apart from the strong noise spikes and makes the riometer data uninformative about the ionospheric radio absorption.

The riometer data taken during the rocket flight did not show any signs of local precipitation. Further inquiry into the periods not covered by the initial data tape may prove useful. More transmitter periods would be available, increasing the data record. The search of the new data would be for small amplitude events, as the data was screened *in situ*, and the available leads from the other instruments have been investigated.

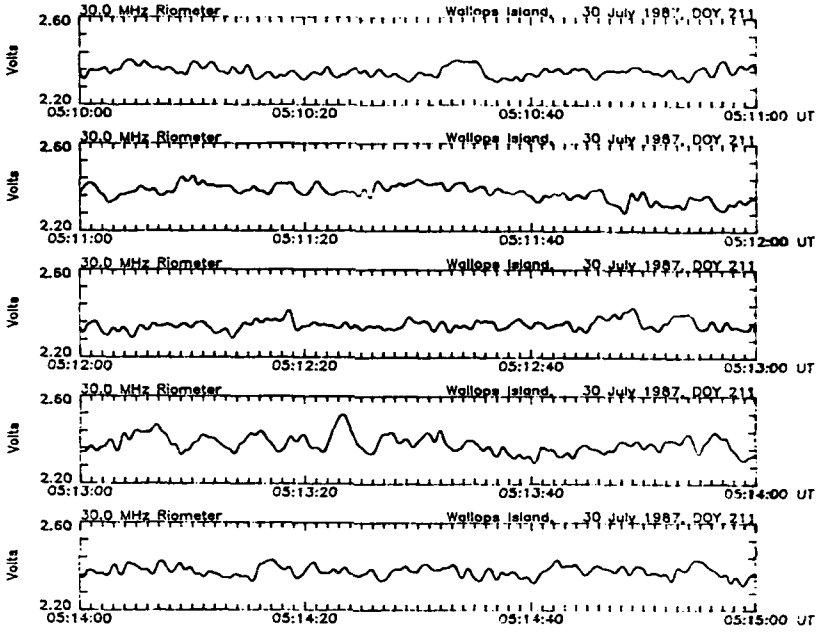

Figure 33. Smoothed data from Figure 32.

THE X-RAY DATA

The integral channel x-ray data was plotted in fifteen minute segments for each of the usable balloon flights. Each of these segments were passed through a low-pass filter at several different cut-off frequencies to eliminate random noise. The low pass filter used was recursive with forwards and backwards passes through the data. The resulting filter had zero phase shift and a nearly square cut-off frequency. The periods that displayed possible counting rate peaks were plotted at increased time resolution. The expanded plots were also filtered with several cut-off frequency values.

The last forty-five minutes of flight #2 apparently had counting rate peaks that lasted longer than seemed to be due to random noise. Particular attention was paid to this period, however the strongest peaks that could be found from either flight were further studied to determine the standard deviation. An example plot is seen in Figure 34. The 50-75 keV channel was plotted in Figure 35 for the same period as Figure 34. The integral channel data from Figure 34 was filtered, and is seen in Figure 36. No sustained counting rate peaks were found to be more than two standard deviations from the mean. The average for flight #1 showed a slight increase towards the end of the

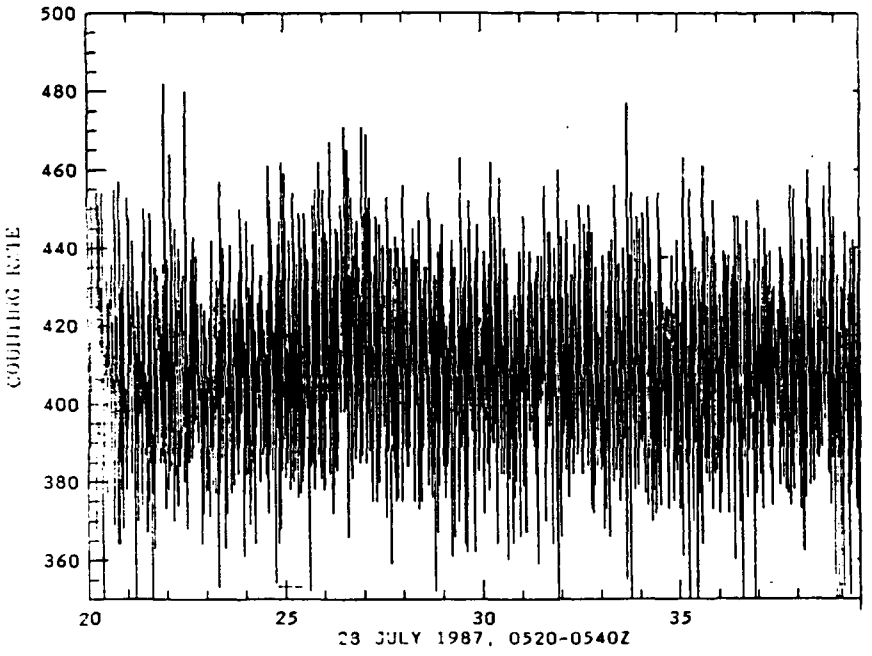

Figure 34. X-Ray Data. Twenty minutes of integral channel data from the end of flight two. This is during the period that the real-time x-ray data seemed to show an elevated counting rate.

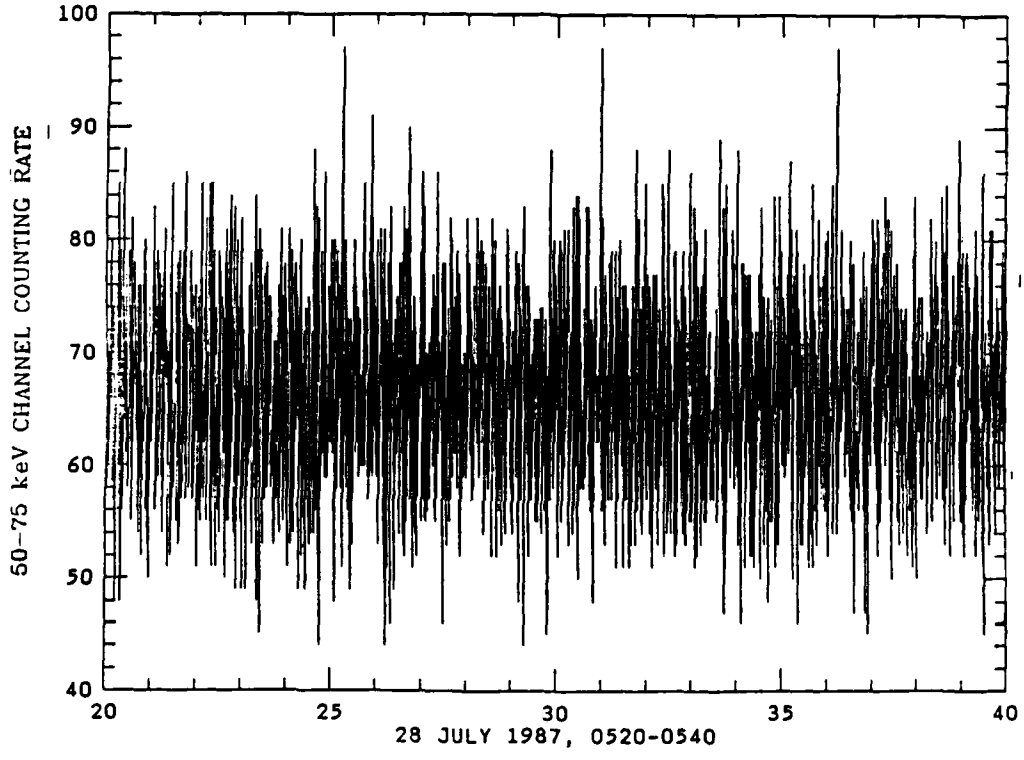

Figure 35. X-Ray Data. Twenty minutes of 50-75keV channel data from the end of flight two. This is during the same period as Figure 34.

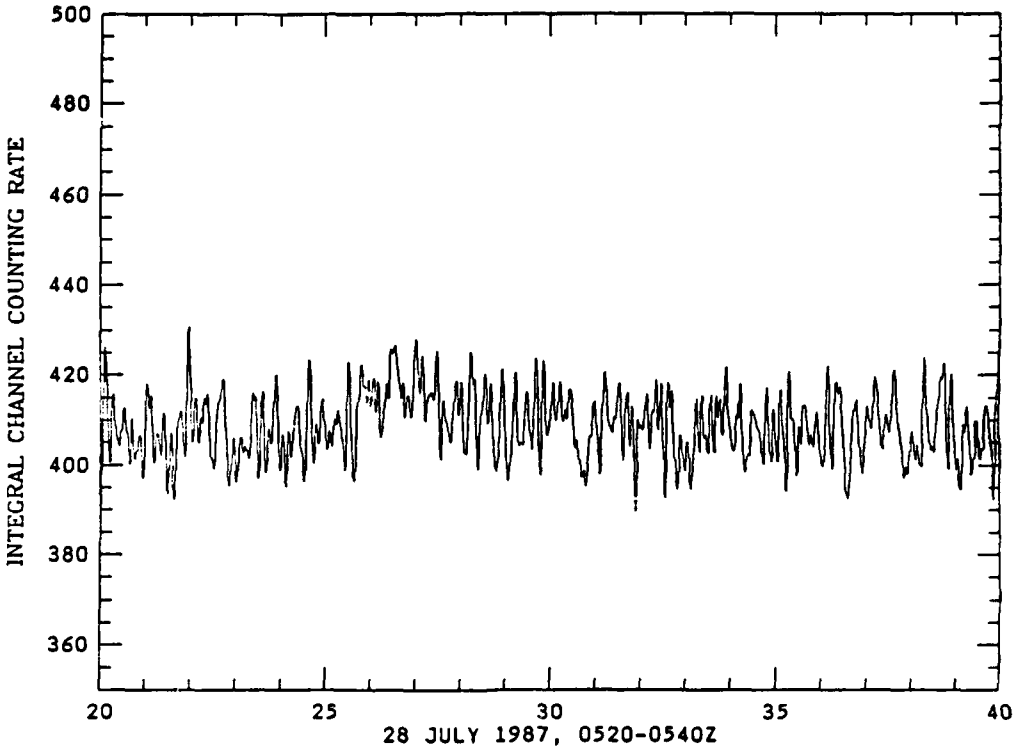

Figure 36. Filtered X-Ray Data. The integral channel data from Figure 34 was run through a low pass filter to eliminate the high level of random noise seen in Figure 34.

flight as is seen in Figure 37a. The average for flight #2 was extraordinarily stable, and did not vary by more than one percent while balloon was at float (Figure 38a).

Histograms of the x-ray counting rates versus the frequency of observations of the counting rates were calculated to further examine the balloon data for deviations from a random background rate. (Figures 37 and 38) Both appear to be a Gaussian distribution. The broad, flat peak for flight #1 (Figure 37b) is due to the gradual shift of the average, and both of the wings of the histogram show tails similar to the wings seen on flight #2 (Figure 38b). If a secondary peak had shown up it would have been evidence of activity not detected by the other methods employed here.

The x-ray data does not appear to contain any evidence of enhanced x-rays observed at the float level. This is evidence for a lack of electron precipitation, electron precipitation with energies below those required to produce x-rays that may penetrate to 38km, or electron precipitation that produced x-rays below the minimum 15KeV detectable by the x-ray detector. The second two cases, those with x-rays undetectable by the balloon, are essentially the same, and are unsupported by evidence for electron precipitation on the other instrumentation deployed under the Wave Induced Particle Precipitation campaign.

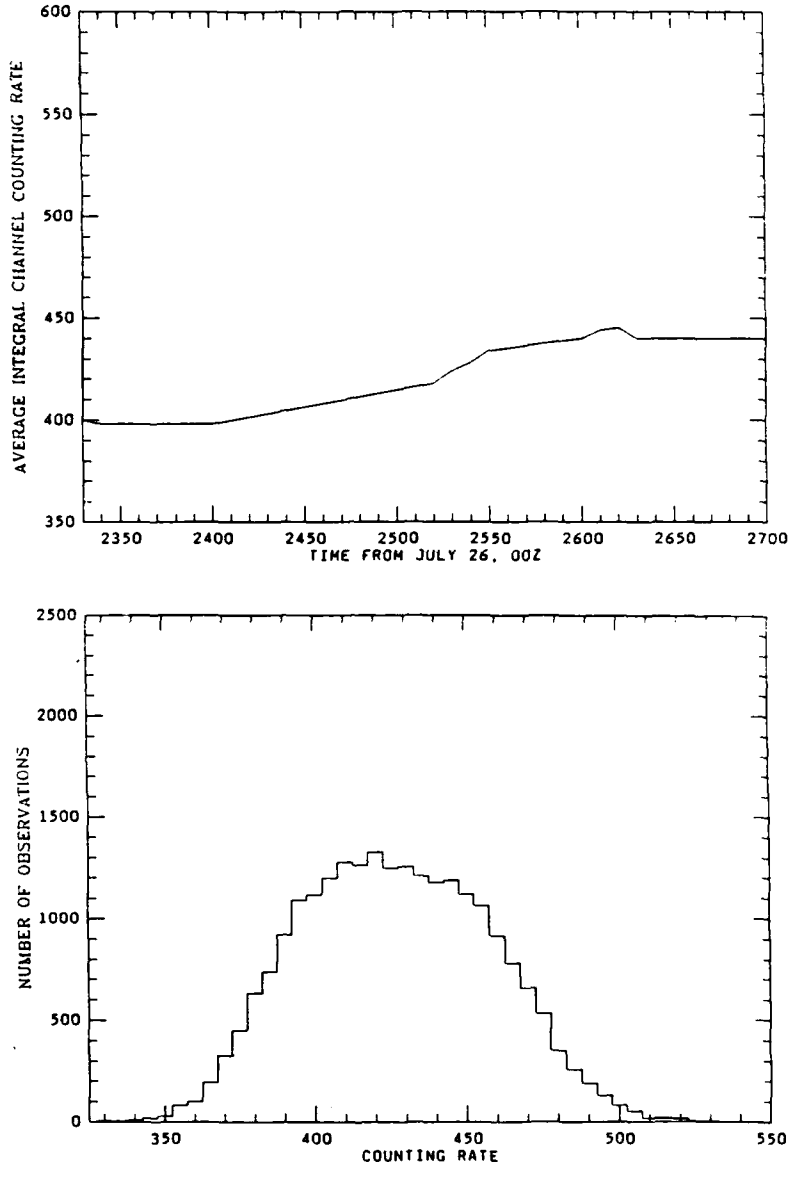

Figure 37. Balloon Flight 1. (a) Plot of the average counting rate for the histogram in b. The gradual increase in averge counting rate is responsible for the wide peak in the histogram. (b) Histogram of Counting Rate Observations for Balloon Flight 1.

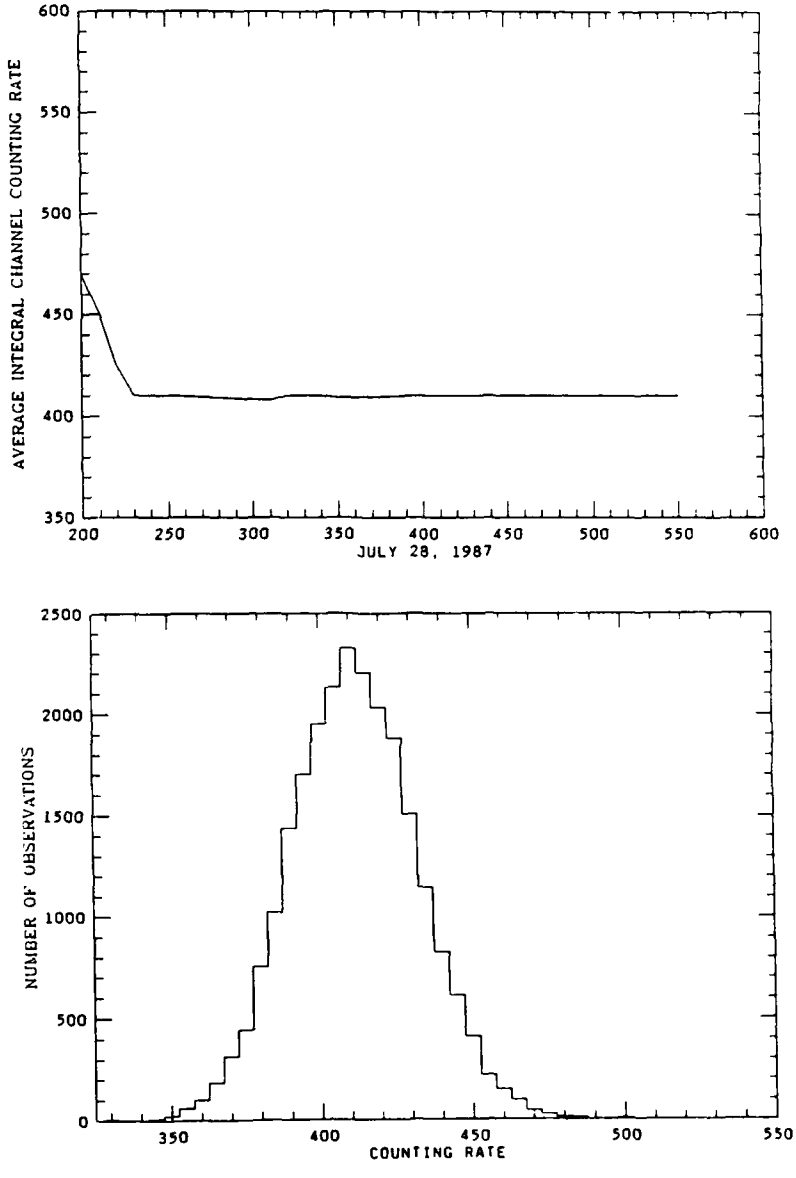

Figure 38. Balloon Flight 2. (a) Plot of the average counting rate for the histogram in b. (b) Histogram of Counting Rate Observations for Balloon Flight 2.

SUMMARY

Both of the balloon flights were over regions of thunderstorms. Frequent lightning was observed on the lightning detector system and the riometer. The positive cloud to ground stroke rate was fairly high, and were verified as strong VLF radio sources by the riometer. The meteorological conditions provided the lightning that was required as a necessary condition for electron precipitation due to lightning.

The x-ray and riometer data did not contain any sign of electron precipitation for any of the methods used. Further investigation of the riometer data might be productive.

CHAPTER 7

SUMMARY AND CONCLUSIONS

SUMMARY

Wave Induced Particle Precipitation was examined. Each of the interactions involved was highlighted.

The role of lightning in the particle precipitation process was discussed. The possible link of particle precipitation with positive cloud to ground lightning strokes generated an examination of the thunderstorm charging process.

In severe and dissipating storms, the positively charged cirrus anvil will be advected well away from the main body of the thunderstorm. If the anvil contains a high enough charge density, a lightning channel will break down along the path from the anvil to the earth's surface. The longer path length requires such a high charge density that a single return stroke is sufficient to discharge the excess charge region. The single stroke carries an order of magnitude more charge, and lasts twice as long as negative cloud to ground.

The radio signal from the positive strokes is much more powerful than the signal from negative strokes. Without further investigation, this would seem to partially

explain the possible correlation between positive strokes and particle precipitation. Another possible explanation is the generation of positive strokes by severe storms. Severe storms produce much more frequent lightning, including some negative cloud to ground strokes that are as powerful as the average positive strokes.

The propagation of the lightning or transmitter produced VLF radio wave is fairly well understood within Earth Ionosphere Waveguide. The penetration of the ionosphere and propagation within the magnetosphere are understood from theory, but the highly variable nature of the ionosphere and the magnetosphere limit our ability to forecast where wave ducting will occur. Whistlers are not observed at nearly the rate that sferics are produced; and the rate of detected whistlers is not directly proportional to the rate of sferic generation. Whistlers are observed, and are not particularly uncommon.

The interaction between the whistlers and plasmaspheric electrons is also understood theoretically, and can be modeled given initial particle energy and density for a whistler on a particular magnetic field line.

Again the upper atmospheric parameters that govern the wave particle precipitation mechanism are not easily available. Satellite measurements are taken, but are not available in real time. The most effective plasmaspheric probe used in the WIPP campaign was the precipitation

mechanism itself. If some precipitation was detected, more would be likely to occur, since plasmaspheric conditions allowed the one burst.

The instruments employed for the WIPP campaign had been used for investigation of similar precipitation events, but the only previous detection of lightning-induced precipitation was from short duration rockets and from low spatial resolution VLF receivers. The other detectors were all relatively long-lived detectors of local events. The rarity of detected events indicated that the local site must be operational for long perids in order for an event to occur overhead.

The failure of two of the balloon payloads, and the operation limitations on the two working payloads significantly reduced the available balloon data. In the case of flight two, another half hour of data would have allowed the correlation of balloon data, and a Trimpi event observed on a VLF reciever.

The available balloon data were analyzed and showed no signs of electron precipitation. Only a portion of the riometer data was available for this study. Further analysis might yield precipitation events. All of the data had been screened already, so any events yet to be found will be on the edge of detectability.

CONCLUSIONS

Lightning sferic-induced particle precipitation has been observed previously. The lack of events detected by this part of the WIPP campaign does not bring the existence of the phenomena into question. The practical problems encountered implies that the null result does not affect the validity of the methods employed. Different experimental methods might have increased the chances of observing a precipitation event. No coordinated campaigns had ever been used to detect particle precipitation, so the problems involved had not been previously encountered.

The relative scarcity of observations points to infrequent and highly localized events. The local detectors need to be used to further examine the electron precipitation. A follow-on campaign might consist of ground based detectors observing for a period of months before the active phase. The presence of large numbers of investigators and support personnel would not be required during this phase.

A second phase where the active experiments, such as balloon and rocket launches and transmitter modulation, would follow. This would be after the ground measurements had been analyzed and some measure of predictability added. The chances of encountering electron precipitation could be maximized for the active experiment. This would allow an informed decision to be made about the duration of the

active experiment, maximizing the presence of the support personnel. The likelihood of a positive result would be optimized, and would give objective evidence for the length of the active experiment.

Further investigation of the link between positive strokes and electron precipitation would be interesting. The possible correlation may be due to positive strokes directly causing the precipitation, or the increased number of strokes associated with severe thunderstorms increasing the number of potential whistlers. The strength of the correlation might allow better forecasts about the likelihood of electron precipitation from readily available weather forecasts.

The wave-induced particle-precipitaion phenomenon links a wide variety of physical processes through large depths in the atmosphere. The wave-particle interaction and the plasmaspheric parameters that control it seem to be the dominant factor in determining whether or not the precipitation occurs. More research needs to be done to discover the areal coverage for an event, and to further study the spectral characteristics of the precipitated electrons.

BIBLIOGRAPHY

Akimoto, K., S. Peter Gray, and N. Omidi, 1987: Electron/Ion Whistler Instabilities and Magnetic Noise Bursts. *Journal of Geophysical Research* 92 (October 1): 11,209-11,214.

Beasley, William, 1985: Positive Cloud-to-Ground Lightning Observations. *Journal of Geophysical Research* 90 (June 30): 6131-6138.

Beasley, William H., Martin A. Uman, Douglas M. Jordan, and Chidambar Ganesh, 1983: Positive Cloud to Ground Lightning Return Strokes. *Journal of Geophysical Research* 88 (October 20): 8475-8482.

Berger, M. J., and S. M. Seltzer, 1972: Bremsstrahlung in the Atmosphere. *Journal of Atmospheric and Terrestrial Physics* 34: 85-108.

Carpenter, D. L., and U. S. Inan, 1987: Seasonal, Latitudinal and Diurnal Distributions of Whistler-Induced Electron Precipitation. *Journal of Geophysical Research* 92 (April 1): 3429-3435.

Cooray, Vernon, and Stig Lundquist, 1982: On the Characteristics of Some Radiation Fields From Lightning and Their Possible Origin in Positive Ground Flashes. *Journal of Geophysical Research* 87 (December 20): 11,203-11,214.

Gaines, E. E., W. L. Imhof, W. E. Francis, M. Walt, and T. J. Rosenberg, 1986: Correlated Electron and X Ray Measurements of Quiet Time Electron Precipitation: A Comparative Study of Bremsstrahlung Production and Transport in the Atmosphere. *Journal of Geophyical Research* 91 (December 1): 13,455-13,462.

Goldberg, R. A., S. A. Curtis, and J. R. Barcus, 1987: Detailed Spectral Structure of Magnetospheric Electron Bursts Precipitated by Lightning. *Journal of Geophysical Research* 92 (March 1): 2505-2513.

Hargreaves, J. K. 1979: *The Upper Atmosphere and Solar-Terrestrial Relations.* New York: Van Nostrand Reinhold Company.

Inan, Umran S., 1987: Gyroresonant Pitch Angle Scattering by Coherent and Incoherent Whistler Mode Waves in the Magnetosphere. *Journal of Geophysical Research* 92 (January 1): 127-142.

Inan, U. S., and D. L. Carpenter, 1987: Lightning-Induced Electron Precipitation Events Observed at L = 2.4 as Phase and Amplitude Perturbations on Subionospheric VLF Signals. *Journal of Geophysical Research* 92 (April 1): 3293-3303.

Krider, E. Philip, and Changming Guo, 1983: The Peak Electromagnetic Power Radiated by Lightning Return Strokes. *Journal of Geophysical Research* 88 (October 20): 8471-8474.

Krishnaswamy. S., D. L. Detrick, and T. J. Rosenberg, 1985: The Inflection Point Method of Determining Riometer Quiet Day Curves. *Radio Science* 20 (January-February): 123-136.

Lanzerotti, L. J., and C. G. Park, ed., 1978: *The Antarctic Research Series. Vol. 29, Upper Atmosphere Research in Antarctica.* Washington, DC: American Geophysical Union.

Le Vine, David M., 1980: Sources of the Strongest RF Radiation From Lightning. *Journal of Geophysical Research* 85 (July 20): 4091-4095.

Liou, Kuo-Nan, 1980: International Geophysics Series. Vol. 26, *An Introduction to Atmospheric Radiation.* Orlando: Academic Press, Inc.

National Academy of Sciences, Panel on the Earth's Electrical Environment, 1986. *Studies in Geophysics: The Earth's Electrical Environment.* Washington, DC: National Academy Press.

Omura, Yoshiharu, and Hiroshi Matsumoto, 1987: Competing Processes of Whistler and Electrostatic Instabilities in the Magnetosphere. *Journal of Geophysical Research* 92 (August 1): 8649-8659.

Orville, Richard E., Ronald W. Henderson, and Lance F. Bosart, 1988: Bipole Patterns Revealed by Lightning Locations in Mesoscale Storm Systems. *Geophysical Research Letters* 15 (February): 129-132.

Ray, Peter S., Donald R. MacGorman, and W. David Rust, 1987: Lightning Location Relative to Storm Structure in a Supercell Storm and a Multicell Storm. *Journal of Geophysical Research* 92 (May 20): 5713-5724.

Rosenberg, T. J., D. L. Detrick, and U. S. Inan. 1988. *Observations and Modeling of Wave-Induced Microburst Electron Precipitation*. College Park, Maryland: University of Maryland, Institute for Physical Science and Technology. Photocopied.

Rosenberg, T. J., and J. R. Dudeney, 1986: The Local Time, Substorm, and Seasonal Dependence of Electron Precipitation at L = 4 Inferred from Riometer Measurements. *Journal of Geophysical Research* 91 (November 1): 12,032-12,040.

Rosenberg, T. J., R. A. Helliwell, and J. P. Katsufrakis, 1971: Electron Precipitation Associated with Discrete Very-Low-Frequency Emissions. *Journal of Geophysical Research* 76 (December 1): 8445-8452.

Rust, W. David, and Donald R. MacGorman, 1981: Positive Cloud-to-Ground Lightning Flashes in Severe Storms. *Geophysical Research Letters* 8 (July): 791-794.

Rust, W. David, William L. Taylor, and Donald R. MacGorman, 1981: Research on Electrical Properties of Severe Thunderstorms in the Great Plains. *Bulletin of the American Meteorological Society* 62 (September): 1286-1293.

Stoker, P. H., 1987: Riometer Absorption and Spectral Index for Precipitating Electrons With Exponential Spectra. *Journal of Geophysical Research* 92 (June 1): 5961-5968.

Tolstoy, A., T. J. Rosenberg, and D. L. Carpenter, 1982: The Influence of Localized Precipitation-Induced D-Region Ionization Enhancements on Subionospheric VLF Propagation. *Geophysical Research Letters* 9 (May): 563-566.

Tolstoy, A., T. J. Rosenberg, U. S. Inan, and D. L. Carpenter, 1986: Model Predictions of Subionosperic VLF Signal Perturbations Resulting From Localized, Electron Precipitation-Induced Ionization Enhancement Regions. *Journal of Geophysical Research* 91 (December 1): 13,473-13,482.

Uman, Martin A., 1985: Lightning Return Stroke Electric and Magnetic Fields. *Journal of Geophysical Research* 90 (June 30): 6121-6130.

Wallace, John M., and Peter V. Hobbs, 1977: Atmospheric Science: *An Introductory Survey*. New York: Academic Press.

CURRICULUM VITAE

Name: Jon Eric Lundberg.

Permanent address: [redacted]

PII Redacted

Degree and date to be conferred: M.S., 1988

Date of birth: [redacted]

Place of birth: [redacted]

Secondary education: Brighton High School
Brighton, New York, 1979

Collegiate education:	Dates	Degree and Date	
University of Virginia	1979-1983	B.A.	1983
North Carolina State U	1983-1984		
University of Maryland	1986-1988	M.S.	1988

Majors: Physics (UVa), Meteorology (NCSU, UMd)

Professional positions held: Region Weather Officer
24th NORAD REGION
Det 8, 26WS
Griffiss AFB, NY, 13440
1984-1986

Environmental Assessment
Officer, Over the Horizon
Backscatter Radar
Bangor ME, 04401
1988